63-3-5

RESEARCH LABORATORY

a division of
AVCO CORPORATION

HYDRODYNAMIC EFFECTS PRODUCED BY PULSE MICROWAVE DISCHARGES

S. C. Lin and G. P. Theofilos

RESEARCH REPORT 138
Contract No. AF 19(604)-7458
October 1962

prepared for
AIR FORCE CAMBRIDGE RESEARCH LABORATORIES
OFFICE OF AEROSPACE RESEARCH
UNITED STATES AIR FORCE
Bedford, Massachusetts

AFCRL-63-126 RESEARCH REPORT 138

HYDRODYNAMIC EFFECTS PRODUCED BY PULSE MICROWAVE DISCHARGES

by

S. C. Lin and G. P. Theofilos

AVCO-EVERETT RESEARCH LABORATORY
a division of
AVCO CORPORATION
Everett, Massachusetts

Project 5561
Task 556112

Contract No. AF 19(604)-7458

October 1962

prepared for

AIR FORCE CAMBRIDGE RESEARCH LABORATORIES
OFFICE OF AEROSPACE RESEARCH
UNITED STATES AIR FORCE
Bedford, Massachusetts

Requests for additional copies by Agencies of the Department of Defense, their contractors, and other Government agencies should be directed to the:

DEFENSE DOCUMENTATION CENTER (DDC)
ARLINGTON HALL STATION
ARLINGTON 12, VIRGINIA

All other persons and organizations should apply to the:

U. S. DEPARTMENT OF COMMERCE
OFFICE OF TECHNICAL SERVICES
WASHINGTON 25, D. C.

ABSTRACT

An elementary theory is developed for predicting the strength of pressure waves to be expected from sudden breakdown of a gas by high frequency electromagnetic waves in a one-dimensional geometry. It is shown that for an uncontrolled breakdown where the local field strength is not carefully matched to the instantaneous plasma condition to avoid strong reflections, the heating effect will be self-limiting and the resultant shock strength depends only on the incident wave frequency and on the initial gas density. Numerical example for microwave breakdown in air indicates that at normal sea level density, the shock wave accompanying the breakdown is generally quite weak (of the order of Mach 1.1 at 100 Gc/S frequency). However, for breakdown at lower air densities, stronger shock waves can be anticipated.

Preliminary experimental observations of pressure waves generated in a one-dimensional channel by pulse microwave discharges tended to confirm the general features of the elementary theory but showed somewhat stronger effects than predicted.

I. INTRODUCTION

In theoretical treatments of high frequency breakdown and microwave discharges,[1,2] the hydrodynamic effects produced by the discharge are usually neglected. While this may be justified in continuous wave discharges where the gas sample involved is in a quasi-steady state, such neglect of the dynamic effects in pulse discharges is open to question on account of possible density modulation by the expansion and mass motion of the gas in the discharge region. From a practical point of view, these hydrodynamic effects could be of some importance in high power communication systems since the breakdown may induce unexpected mechanical loads on the surrounding structures. In gasdynamics and in astrophysics, a complementary problem of possible interest is the question of whether it is possible to produce strong shock waves from a distance by intense bursts of electromagnetic waves.

In a recent paper, Musson-Genon and Brousseau[3] have reported some optical observations of shock waves produced by microwave pulses within the switching tubes (or TR tubes) in a duplexer. Using He, Ne, Ar and Xe at initial pressure between 10 and 50 mm Hg as filling gases for the switching tubes (glass tubes of 1.8 to 7.2 mm diameter and 40 to 80 mm length, inserted perpendicularly through the middle of a rectangular wave guide, which formed part of the duplexer), and peak power varying between 33 and 200 kw (1 μsec pulse width, and 10^3 pulses/sec repetition rate, at some unspecified microwave frequency), shock waves of apparent Mach number between 1.01 and 2.00 have been

observed to propagate transversely across the diameter and subsequently reflect back from the opposite side of the switching tube. No attempt has been made, however, to interpret these experimental results on a quantitative basis.

In the present paper, we shall try to estimate the theoretical shock strength to be expected from pulsed discharges of this type from an elementary theory, and to examine the various factors which govern the strength of the shock wave thus produced. For simplicity, the theoretical analysis will be based on a one-dimensional geometry, and attention will be paid only to the question of the initial shock formation. The more complicated problem of subsequent wave motion and reflections from the boundaries of a finite geometry will be avoided. Numerical results will be given for the case of microwave breakdown in air as functions of wave frequency and initial density. These results will also be compared with some preliminary experiments on shock wave generation in a one-dimensional channel by pulsed microwave discharges.

II. ELEMENTARY THEORY

It is well known that when energy is suddenly deposited non-uniformly in a gas, the regions of high energy deposition will expand against the regions of lower energy deposition, and hence wave motions will be developed. In a one-dimensional situation where the energy deposition is confined to a slab of thickness L in an otherwise undisturbed gas, and the time of energy deposition is short compared with the time it takes acoustic waves to traverse the distance L, the resultant shock strength can be estimated from the usual shock tube formula:[4]

$$M_1^2 = \frac{\gamma-1}{2\gamma} - \frac{\gamma+1}{2\gamma}\left(1+\frac{\overline{\Delta E}}{E_1}\right)\left[1 - \frac{\gamma-1}{\gamma+1}\frac{M_1^2-1}{M_1\left(1+\frac{\overline{\Delta E}}{E_1}\right)^{\frac{1}{2}}}\right]^{\frac{2\gamma}{\gamma-1}} \quad (1)$$

where M_1 denotes the shock Mach number (shock velocity divided by the speed of sound of the undisturbed gas); γ is the specific heat ratio of the gas; $E_1 = kT_1/(\gamma - 1)$ is the mean initial thermal energy per gas molecule; and $\overline{\Delta E}$ is the mean energy deposition per molecule within the slab L. For small values of $\overline{\Delta E}/E_1$, it is more convenient to expand M_1 into a series in ascending powers of $\overline{\Delta E}/E_1$ so that Eq. (1) may be replaced by

$$M_1 = 1 + \frac{\gamma+1}{8\gamma}\left(\frac{\overline{\Delta E}}{E_1}\right) - \frac{(\gamma+1)(3\gamma-1)}{128\gamma^2}\left(\frac{\overline{\Delta E}}{E_1}\right)^2 + \frac{(\gamma+1)(23\gamma^2-10\gamma-1)}{512\gamma^3}\left(\frac{\overline{\Delta E}}{E_1}\right)^3 + \cdots\cdots \quad (1a)$$

A plot of $M_1 - 1$ verses $\overline{\Delta E}/E_1$ according to Eq. (1) or (1a) for γ = 5/3 (ideal monatomic gas), 7/5 (diatomic gas) and 6/5, respectively, is illustrated in Fig. 1. It is seen that the shock strength $M_1 - 1$ varies almost linearly with $\overline{\Delta E}/E_1$, and is surprisingly insensitive to the specific heat ratio γ.

The problem under consideration is now reduced to the problem of determining the energy deposition $\overline{\Delta E}$ by the pulse discharge. Since

the electromagnetic field energy is deposited into the gas mainly through the motion of the free electrons, we may write, for the total energy transferred per unit volume,[5]

$$n_1 \overline{\Delta E} = \int_\tau \int_{\vec{c}_e} \int_{\vec{c}_\xi} \int_0^{2\pi} \int_0^\infty n_e f_e \sum_\xi n_\xi f_\xi \cdot \Delta E_{e\xi}\, g_{e\xi}\, b\, db\, d\epsilon\, d\vec{c}_\xi\, d\vec{c}_e\, dt \qquad (2)$$

where n_1 is the total number density of molecules in the initial gas mixture; n_e, n_ξ, and f_e, f_ξ are, respectively, the instantaneous number densities and velocity distribution functions of the free electrons and of the type-ξ molecule in the gas mixture during the discharge; $\Delta E_{e\xi}$ is the amount of energy transferred for a collision between an electron of velocity $\vec{c}_e$ and a type-ξ molecule of velocity $\vec{c}_\xi$ at impact parameter b and impact plane angle ϵ; and $g_{e\xi}$ is the relative speed between the electron and the molecule before the collision. The integrations over $\vec{c}_e$ and $\vec{c}_\xi$ are to be extended over the appropriate velocity spaces, and the integration over time is to be extended over the duration of the pulse discharge. The above expression may be considered quite exact if the energy transferred from the electron to all possible energy states of the molecule is accounted for in the expression for $\Delta E_{e\xi}$. However, in the absence of sufficiently detailed information on molecular properties, it is necessary to replace the energy transfer integral by appropriate macroscopically observed quantities. This can be accomplished,

for example, by defining an averaged fractional energy loss Λ for the electron-molecule collisions, such that

$$\int_{\vec{c}_e}\int_{\vec{c}_s}\int_0^{2\pi}\int_0^{\infty}\sum_s n_s f_s \Delta E_{es}\, g_{es}\, b\,db\,d\epsilon\, d\vec{c}_s\, d\vec{c}_e \equiv (E_e - E)\,\nu_c\,\Lambda \tag{3}$$

where

$$E_e \equiv \int_{\vec{c}_e} \frac{1}{2} m_e c_e^2 f_e\, d\vec{c}_e \ , \tag{4}$$

$$E \equiv \frac{kT}{\gamma - 1} \tag{5}$$

are, respectively, the instantaneous mean energies for the free electrons and for the molecules (T being the gas temperature), and ν_c is the total electron-molecule collision frequency (per electron per unit time). For want of more precise information, one may tentatively identify Λ with the fractional energy loss coefficient that can be determined, for example, from electron swarm experiments.[6] In terms of these macroscopic quantities, Eq. (2) becomes simply,

$$n_1 \overline{\Delta E} = \int_{\tau} (E_e - E) \nu_c \Lambda n_e \, dt \tag{6}$$

A further simplication can now be made by noting that during the discharge, E_e is generally much greater than E, and that E_e, ν_c, Λ only vary slowly with time during the discharge. One may replace these quantities by appropriate time-averaged quantities, such that

$$n_1 \overline{\Delta E} = \overline{E_e}\, \overline{\nu_c}\, \overline{\Lambda} \int_{\tau} n_e \, dt \tag{7}$$

If the duration of the discharge τ is so short, or the geometrical dimension under consideration is so large, that diffusion losses can be neglected, then the instantaneous electron balance equation may be written as,

$$\frac{dn_e}{dt} = n_e \nu_i - n_e \nu_a - \alpha n_e^2 \tag{8}$$

where ν_i and ν_a are, respectively, the ionizing collision frequency and attachment frequency per electron; and α is the volume recombination coefficient for the electrons and ions. Note that ν_i, ν_a and α are all functions of the mean electron energy E_e and the electron velocity distribution function f_e, which, in turn, depend on the strength and frequency of the applied electromagnetic field. The minimum field strength required to maintain the discharge is given by the

condition that $\frac{dn_e}{dt}$ vanishes, or

$$\nu_i = \nu_a + \alpha n_e \tag{9}$$

Due to the existence of a threshold ionization potential of the order of 10 volts for most gases and the absence of comparable activation energies for the attachment and recombination processes, the ionizing collision frequency ν_i is generally a much steeper function of the electron energy than are ν_a and α under typical gas discharge conditions (see numerical example in Section III). Therefore, in an uncontrolled discharge where the applied field strength is not carefully regulated to satisfy Eq. (9) at all times, one may expect to find a considerable fraction of the discharge period τ during which the field strength is appreciably in excess of the minimum breakdown field strength, such that

$$\nu_i >> \nu_a + \alpha n_e \tag{10}$$

During this time, the electron balance equation (8) becomes simply

$$\frac{dn_e}{dt} \cong n_e \nu_i \tag{8a}$$

Substitution of the above expression into (7) yields,

$$n_1 \overline{\Delta E} \cong \overline{E_e}\, \overline{\nu_c}\, \overline{\Lambda} \int_{\tau} \frac{dn_e}{\nu_i} \tag{7a}$$

In a microwave discharge, the discharge region is connected to the source of rf energy either through waveguides or appropriate free-space propagation paths (as in a focused discharge). As the electron density in the discharge region builds up toward the critical value corresponding to plasma resonance at the incident wave frequency f,

$$n_e^* = (\pi m_e / e^2) f^2 \tag{11}$$

(m_e and e being the electron mass and charge, respectively) the propagation paths will be interrupted by strong reflections at the boundaries so that no further substantial heating of the discharge region can be accomplished by the electromagnetic wave.[7] In other words, there exists a natural cutoff for Eq. (7a) at the critical electron density n_e^*, irrespective of the magnitude and duration of the rf pulse. This leads to the following approximate expression for the amount of energy deposition in the gas that can be accomplished by an uncontrolled pulse microwave discharge.

$$\overline{\Delta E} \cong \overline{E_e} \Lambda \frac{\overline{\nu_c}}{\overline{\nu_i}} \frac{n_e^*}{n_1} \tag{12}$$

Here $\overline{\nu_i}$ represents an appropriate time-averaged value for the ionizing collision frequency during the electron density build-up period. It is interesting to note from this simple expression that high field intensity beyond that required for breakdown tends to discourage energy deposition in the gas (since ν_i increases rapidly with field strength). Another interesting but perhaps obvious conclusion which one may draw

from Eqs. (11) and (12) is that at a fixed wave frequency f, the specific energy deposition $\overline{\Delta E}$ decreases with increasing molecular density, n_1. At a fixed density, the energy deposition is expected to increase roughly as the square of the wave frequency.

III. EXAMPLE OF MICROWAVE DISCHARGE IN AIR

As a numerical example, the mean electron energy E_e, the ionizing collision frequency ν_i, the attachment frequency ν_a, and the non-ionizing collision frequency ν_c at minimum breakdown power density are plotted in Figs. 2, 3, and 4 as functions of microwave frequency f and initial air density ρ_1 (ρ_o being the standard atmospheric density at sea level). The minimum breakdown power density, which is defined as the power density at which Eq. (9) is satisfied for $n_e = 0$, is plotted in Fig. 5. The approximate kinetic equations and molecular data employed in obtaining these results are given in Appendix A. It suffices to mention here that even though the method employed was quite crude and the molecular data uncertain, the breakdown power density is in order-of-magnitude agreement with those obtained by others using different methods.[2,8] As a measure of the relative sensitivity of the ionizing collision frequency ν_i and the attachment frequency ν_a to the microwave power density P, the logarithmic derivatives of ν_i and ν_a with respect to P at the minimum breakdown power density are plotted in Fig. 6 as functions of frequency and air density.

Because of the relatively sharp dependence of ν_i on P, the limiting energy deposition per air molecule in an uncontrolled pulse microwave discharge is roughly given by Eq. (12), with the averaged quantities $\overline{E_e}$, $\overline{\Lambda}$, $\overline{\nu_c}$, and $\overline{\nu_i}$ replaced by their respective values

at the minimum breakdown power density. Using values of $(E_e)_{B.D.}$, $(\nu_c)_{B.D.}$, and $(\nu_i)_{B.D.}$ shown in Figs. 2, 3, and 4, and the energy loss coefficient Λ represented by the dotted curve in Fig. A-1, the limiting energy deposition $\overline{\Delta E}$ calculated according to Eq. (12) is shown in Fig. 7 as a function of wave frequency and initial air density. From this, one can calculate the resultant shock strength M_1-1 according to Eq. (1) for γ = 7/5 and $E_1 = 6.3 \times 10^{-2}$ electron-volts (i.e., diatomic gas at room temperature). The shock strength so obtained is plotted in Fig. 8 (solid curves).

The theoretical results shown in Figs. 7 and 8 indicate that for uncontrolled microwave breakdown in air at normal sea level density, the hydrodynamic effects accompanying the breakdown would generally be quite weak. For example, even at the highest frequency considered ($f = 10^{11}$ cycles/sec., or 3 mm free space wavelength), the Mach number of the shock wave produced would only be of the order of 1.1. However, at lower air densities, it appears possible to produce stronger shock waves by microwave discharges.

IV. DESCRIPTION OF PRELIMINARY EXPERIMENT

In a first attempt to produce measurable hydrodynamic disturbances from pulse microwave discharges in the laboratory and to verify in a semi-quantitative manner the elementary theory just described, the following experiment was performed.

The experimental arrangement is schematically shown in Fig. 9, and photographically illustrated in Figs. 10(a), (b) and (c). This experiment essentially consisted of breaking down a gas by repetitive microwave pulses at the end of a non-conducting one-dimensional channel (or

shock tube) and observing the propagation of hydrodynamic disturbances downstream by a pressure transducer. The microwave pulses were provided by a Raytheon QK-624 magnetron operating at X-band frequency (i.e., f $\cong$ 10 Gc/S, or 10^{10} cycles/sec). The modulator and power supply required to operate the magnetron were taken from a surplus APS-20B radar set, which allowed the peak pulse power to be varied conveniently between 10^5 and 10^6 watts at a pulse width of about 2 μsec and a repetition rate of about 200 pulses/sec. The microwave power from the magnetron is transmitted to the shock tube through a standard RG-51 rectangular waveguide, a ferrite circulator (which allowed the reflected power from the breakdown region to be dissipated harmlessly in an air-cooled dummy load), and a resonance window. Sampling of the incident and the reflected power and pulse shape was accomplished through a cross-guide directional coupler with appropriate attenuators. To avoid premature breakdown in the waveguide, the entire transmitting circuit was pressurized by nitrogen to a pressure of about 3 atmospheres.

The non-conducting shock tube, which was fabricated from lucite bar stock, had interior dimensions identical to those of the RG-51 waveguide (i.e., 2.85 cm x 1.26 cm) and was about 62 cm long. To minimize impedance mismatch, the upstream end of the shock tube was coupled to the waveguide through a pyramidal horn. (The shock tube was shape-fitted and cemented to the inside of the horn as illustrated in Fig. 9). To minimize multiple shock reflections, the downstream end of the shock tube was exhausted into a large vacuum tank.

In a typical experiment, the sample gas (air) was continuously fed into the shock tube through a small orifice located near the resonance window, and was continuously pumped out through the end of the vacuum tank so as to maintain a fresh gas sample in the discharge zone for the successive pulses. The pump-out rate was balanced against the inflow rate through adjustment of a throttling valve until the desired initial pressure in the system was reached. The initial pressure was measured by an alphatron vacuum gage (National Research type 520), and the pressure reading was always taken before the magnetron was switched on. The experiment was started by turning on and raising the magnetron power until breakdown occurred at the upstream end of the lucite shock tube, which manifested itself by a glowing light near the resonance window, and a steady buzzing noise. Pressure disturbances produced by the breakdown were then measured by a statically-calibrated piezo-electric transducer (Kistler type 401, with Model 568 charge amplifier) which was mounted at various fixed distances downstream from the resonance window.

A typical set of oscillograms from the pressure transducer output is illustrated in Figs. 11(a) and (b). The initial air pressure in this case was 450 $\pm$ 50 mm Hg (i.e., $\rho_1/\rho_o \cong 0.6$), and the onset of breakdown was observed to occur at about 2×10^5 watts peak pulse power. The axial distance x between the transducer and the resonance window is marked on the left of each pair of oscillograms. The left hand column of oscillograms in Figs. 11(a) and 11(b) was taken at a writing speed of 100 and 200 μ-sec/cm, respectively, and was triggered directly by the microwave pulse without time delay. They

represent, therefore, the full time history of the transducer output. The right hand column of oscillograms in Figs. 11(a) and 11(b), on the other hand, was taken at a writing speed of 20 μ-sec/cm with appropriate time delay to magnify the main part of the pressure pulse marked by time t_s on the left hand oscillogram in each case. It should be made clear that all these oscillograms were taken in time sequence with a single pressure transducer and hence do not represent the simultaneous record of the transducer output at different distances down the shock tube. In fact, upon close examination, it may be noted that each of these oscillograms was a result of superposition of several consecutive pulses. Because of the apparent reproducibility of the transducer output, one may deduce the averaged propagation history of the pressure disturbance down the shock tube from such a sequence of oscillograms.

A typical plot of the time of arrival of the main pressure disturbance t_s as a function of axial distance x from the resonance window is given in Fig. 12. It is seen that the experimental points can be fitted closely by a straight line passing through the origin. The apparent propagation velocity of the disturbance as given by the slope of the straight line, $U_s = \Delta x/\Delta t_s$, was found to be typically a few percent greater than the speed of sound in air at room temperature, $a_1 = 3.44 \times 10^4$ cm/sec. In view of the fact that the speed of sound in lucite is approximately five times greater, it is quite clear that the main pulse in the transducer output must have been due to a weak shock wave in the gas, even though some of the disturbances which arrived at the transducer before t_s may be attributable to propagation of elastic waves in lucite.

The apparent shock strength

$$M_1 - 1 = (U_s - a_1)/a_1 \tag{13}$$

as obtained from propagation velocity measurment of the main pressure pulse just described is plotted in Fig. 8 as open circles. Each plotted point represents the geometric mean value from a large number of runs (of the order of 10) at a fixed initial air pressure but at different peak microwave power. The vertical bar indicates the maximum spread of each group of experimental points, which showed no systematic variation when the microwave power was varied between the minimum value required for breakdown and five times the minimum value. (The microwave pulse width τ was held at 2 μ-sec.)

An alternative shock strength measurement can be obtained from the amplitude of the calibrated pressure transducer output. Since the pressure rise across a normal shock Δp is related to the shock Mach number M_1 by the well known expression,[9]

$$\frac{\Delta p}{p_1} = \frac{2\gamma}{\gamma+1}(M_1^2 - 1) \tag{14}$$

where p_1 is the initial pressure ahead of the shock, one may write for weak shock waves,

$$M_1 - 1 \cong \frac{\gamma+1}{4\gamma}\frac{\Delta p}{p_1} \tag{15}$$

The shock strength obtained by this alternative method is plotted in Fig. 8 as solid circles.

The two sets of experimental points plotted in Fig. 8 show a factor of 3 discrepancy between the mean shock strength determined from the two different methods. This is not too surprising since in calculating the shock strength according to Eq. (13) with $a_1 = 3.44 \times 10^4$ cm/sec, we have in effect neglected the mean fluid motion due to continuous circulation of the sample gas in the shock tube, as well as all the residual transient effects caused by the repetitive pulses. The neglect of these effects all tended to overestimate the shock strength. Therefore, the true shock strength is probably much closer to that obtained from the pressure measurements (solid points), even though the finite rise time of the transducer might have somewhat underestimated the peak pressure rise across the shock.

These measurements have not yet been extended to lower initial air densities on account of the marginal signal-to-noise ratio of the available pressure transducer.

V. DISCUSSIONS

The preliminary experimental results reported in the preceding section tended to confirm that the hydrodynamic effects accompanying uncontrolled microwave breakdown in air at or near sea level density are generally quite weak and power-independent. However, the absolute magnitude of the observed shock strength turned out to be about a factor of 10 greater than that predicted by the elementary theory, using tentative molecular data (see Appendix A). It is not clear at this time if the discrepancy was mostly due to the inadequacy of the elementary theory, or due to uncertainties in the molecular data (in particular, the fractional energy loss coefficient Λ).

It may also be pointed out that the minimum microwave power density required for breakdown in the experiment appeared to be very much smaller than the theoretical value given in Fig. 5 (by a factor of almost 100, if the full aperture of the rectangular waveguide were used to calculate the power density). The low breakdown power required in the experiment, which was undoubtedly due to the existence of strong local fields near the aperture of the resonance window, may have also contributed significantly to the discrepancy between the observed and predicted shock strength.

In view of the linear dependence of the energy deposition $\overline{\Delta E}$ on the fractional energy loss coefficient Λ (see Eq. (12)) and the fact that the value of Λ for noble gases is generally much smaller than that for air in the range of electron energy under consideration, the apparent shock Mach number of up to 2.00 reported by Musson-Genon and Brousseau[3] for breakdown of He, Ne, Ar and Xe in switching tubes appeared to be somewhat high. On the other hand, the clearly three-dimensional geometry employed in their experiment (with all dimensions comparable to, or smaller than, the free space wavelength) might have favored the formation of stronger shocks than would be possible in a quasi-one dimensional geometry.

The existence of certain basic relationships between the hydrodynamic effects accompanying a microwave breakdown and the energy transfer properties between the electrons and the molecules suggests that basic molecular data and transport properties may be obtained through proper observation of the hydrodynamic effects produced by the breakdown. Even though care must be exercised to make the experimental

geometry conform to the theoretical geometry in comparing the quantitative results, the problem does not appear to be a fundamentally difficult one.

ACKNOWLEDGMENT

This work was supported by the Electronics Research Directorate of the Air Force Research Division, Air Research and Development Command, under Contract AF 19(604)-7458.

APPENDIX A

APPROXIMATE KINETIC EQUATIONS AND MOLECULAR DATA EMPLOYED IN AIR DISCHARGE CALCULATIONS

The ionizing collision frequency ν_i , electron-attachment frequency ν_a , and the non-ionizing collision frequency ν_c were all calculated from a zeroth-order collision integral of the form,

$$\nu_j = 4\pi n_1 \int_0^\infty f_e^{(0)} Q_j(c_e) c_e^3 \, dc_e \tag{A1}$$

where $f_e^{(0)}$ is the zeroth-order electron speed distribution function; $Q_j(c_e)$ is the total cross section (averaged over angular momentum, direction of impact and chemical species) for the process identified by the subscript j (i.e., j = i, a, or c) at electron speed c_e; and

$$n_1 = 2.5 \times 10^{19} \frac{\rho_1}{\rho_0} \tag{A2}$$

is the number density of air molecules at mass density ρ_1 (ρ_0 being the mass density at sea level).

For the electron speed distribution function, we used Margenau's zeroth-order distribution for the field-dominant case:[10]

$$f_e^{(o)} = A_o \exp\left[-\frac{3m_e^3 (c_e^4 + 2\omega^2 \ell^2 c_e^2)}{2m_M e^2 \mathcal{E}^2 \ell^2}\right] \tag{A3}$$

where $\omega = 2\pi f$ is the angular wave frequency; ℓ is the electron mean free path; and $\mathcal{E}$ is the electric field amplitude of the incident wave. Note that Margenau's theory was based on perfectly elastic collisions, while in the present problem, most of the collisions between the electrons and the air molecules would be inelastic (i.e., rotational and vibrational excitation, as well as excitation to the low-lying electronic states of the molecules). To allow for the effects of these inelastic collisions on the distribution function, we have simply replaced the actual mass of the molecule m_M in Eq. (A3) by a considerably smaller "effective mass" m_M'.

The normalization constant A_o is to be determined, as usual, from the condition that

$$4\pi \int_0^\infty f_e^{(o)} c_e^2 \, dc_e = 1 \tag{A4}$$

In terms of the energy parameters introduced by Margenau,[10]

$$\epsilon_1 \equiv \frac{1}{2} m_e \omega^2 \ell^2 \tag{A5}$$

$$\epsilon_2 \equiv e \mathcal{E} \ell \tag{A6}$$

and a non-dimensional velocity

$$u \equiv \left(\frac{3m_e}{2m'_M}\right)^{\frac{1}{4}} \left(\frac{m_e}{\epsilon_2}\right)^{\frac{1}{2}} c_e \tag{A7}$$

Eq. (A3) becomes,

$$f_e^{(o)} = A_o \exp\left[-\left(u^4 + \sqrt{24\frac{m_e}{m'_M}}\,\frac{\epsilon_1}{\epsilon_2}\,u^2\right)\right] \tag{A3'}$$

By treating m'_M, and consequently

$$\xi \equiv \left(\frac{24m_e}{m'_M}\right)^{\frac{1}{2}} \frac{\epsilon_1}{\epsilon_2} \tag{A8}$$

as a constant (which is consistent with Margenau's constant mean-free-path approximation) and substituting (A3') into (A4), we obtain

$$A_o = \left(\frac{3m_e}{2m'_M}\right)^{\frac{3}{4}} \left(\frac{m_e}{\epsilon_2}\right)^{\frac{3}{2}} \Big/ 4\pi I_2(\xi) \tag{A9}$$

where

$$I_2(\xi) \equiv \int_0^\infty \exp\left[-(u^4 + \xi u^2)\right] u^2 du \tag{A10}$$

From these, one can calculate the mean thermal energy of the electron,

$$E_e \equiv 4\pi \int_0^\infty \left(\frac{1}{2} m_e c_e^2\right) f_e^{(0)} c_e^2 \, dc_e$$

$$= \left(\frac{m_M'}{6m_e}\right)^{\frac{1}{2}} \frac{I_4(\xi)}{I_2(\xi)} \epsilon_2 \qquad \text{(A11)}$$

where

$$I_4(\xi) \equiv \int_0^\infty \exp\left[-(u^4 + \xi u^2)\right] u^4 \, du \qquad \text{(A12)}$$

The non-dimensional integrals $I_2(\xi)$ and $I_4(\xi)$ are plotted in Fig. A3 for convenient reference.

To determine the effective mass m_M', one may make the following observation: In the Chapman-Enskog expansion (on which Margenau's theory was based) the collision term involving the mass ratio m_e/m_M was due to the change in magnitude of the electron velocity vector after an elastic collision (see for example, p. 349-350 of Reference 5). In an inelastic collision, the corresponding fractional change in magnitude of the velocity vector would be given by one-half the fractional loss of electron kinetic energy Λ (assuming isotropic scattering) instead of by the mass ratio m_e/m_M. Therefore, as far as the electron motion is concerned, an inelastic collision involving a fractional energy loss Λ has the same effect as an elastic collision with a

molecule of mass

$$m'_M = 2m_e/\Lambda \tag{A13}$$

The average fractional energy loss for electron-molecule collisions in air, N_2 and O_2 has been determined from electron swarm experiments as a function of the mean electron energy by Townsend and Bailey, Huxley and Zaazou, and others.[6] The results are reproduced here in Fig. A1. It is seen that Townsend and Bailey results agreed quite well with the N_2, O_2 data, but Huxley and Zaazou's results fell considerably lower (by a factor of about 10) than the N_2, O_2 data at electron energies above 2 ev. In spite of this apparent discrepancy, all measured value of Λ fell above the elastic-collision limit by a large factor even at the lowest electron energy. In our calculations, a simple analytic curve (dotted curve shown in Fig. A1) which was fitted heavily toward Townsend and Bailey's data was used.

By applying Eq. (A13) to Eqs. (A8) and (A11), and ignoring the difference between the averaged electron energy as defined by Eq. (A11) and the mean electron energy as defined in the swarm experiment, we now obtain the following implicit functional relationship among the mean electron energy E_e, the field strength ξ, the angular wave frequency ω, and the electron mean-free-path ℓ:

$$E_e = \frac{e\xi\ell}{\sqrt{3\Lambda(E_e)}} \frac{I_4(\xi)}{I_2(\xi)} \tag{A14}$$

where

$$\xi \equiv \frac{m_e \omega^2 \ell}{e \mathcal{E}} \sqrt{3\Lambda(E_e)} \qquad \text{(A15)}$$

The mean-free-path ℓ , which is to be treated here as a constant, is simply given by,

$$\ell = (n_1 Q_c)^{-1} \qquad \text{(A16)}$$

where Q_c is the total cross section for electron-air molecule collisions. Within the range of electron energy of interest, one may take (see for example, Fig. 101, p. 206 of Reference 6),

$$Q_c \cong 10^{-15} \qquad cm^2 \qquad \text{(A 17)}$$

Combining (A2), (A16) and (A17), one obtains,

$$\ell \cong 4 \times 10^{-5} (\rho_1 / \rho_0)^{-1} \quad cm \qquad \text{(A18)}$$

For an underdense plasma (i.e., $n_e << n_e^*$), the electric field amplitude $\mathcal{E}$ is related to the power density P through the free space impedance Z_o = 377 ohms, such that,[7]

$$\mathcal{E} \cong (Z_o P)^{\frac{1}{2}} \qquad \text{(A19)}$$

With the aid of Eqs. (A18), (A19), and Fig. (A-1), the implicit equations (A14) and (A15) can be used to determine the mean electron energy E_e as a function of the power density P, the wave frequency f, and the initial air density ρ_1/ρ_o.

Similarly, the various collision frequencies as defined by Eq. (A1) can be calculated from the corresponding cross sections as functions of P, f, and ρ_1/ρ_o. From these, the power density and other quantities of interest at breakdown can, in turn, be calculated as a function of wave frequency and air density from the breakdown condition defined by Eq. (9) in the main text.

In our calculations, the electron-impact ionization cross section Q_i was taken from Table III, p. 265 of Reference 6. The electron attachment cross section Q_a was based on Harrison and Geballe's[11] measurement in O_2 (i.e., the dash-dot curve shown in Fig. A2).

REFERENCES

1. L. Gould and L. W. Roberts, J. Appl. Phys., 27, 1162 (1956).

2. A. D. MacDonald, Proc. I. R. E., 47, 436 (1959).

3. R. Musson-Genon and M. Brousseau, "Ondes De Choc Produites Par Des Impulsions Hyperfrequences Dans Des Tubes De Commutation," Proc. 5th International Conf. on Ionization Phenomena in Gases, H. Maecker, ed., North-Holland, Amsterdam (1962).

4. E. L. Resler, S. C. Lin, and A. R. Kantrowitz, J. Appl. Phys. 23, 1390 (1952).

5. S. Chapman and T. G. Cowling, "The Mathematical Theory of Non-Uniform Gases," Cambridge Univ. Press, London (1952).

6. H. S. W. Massey and E. H. S. Burhop, "Electronic and Ionic Impact Phenomena," Oxford-Clarendon, London (1952), Chapt. IV.

7. J. A. Stratton, "Electromagnetic Theory," McGraw-Hill (1941), Chapts. V and IX.

8. N. Kroll, "Memorandum on Microwave Breakdown," Institute for Defense Analyses, Jason Division Report (1961).

9. See for example, H. W. Liepmann and A. E. Puckett, "Introduction to Aerodynamics of a Compressible Fluid," John Wiley & Sons, N. Y. (1947), p. 40.

10. H. Margenau, Phys. Rev. 69, 508 (1946).

11. M. A. Harrison and R. Geballe, Phys. Rev. 91, 1 (1953).

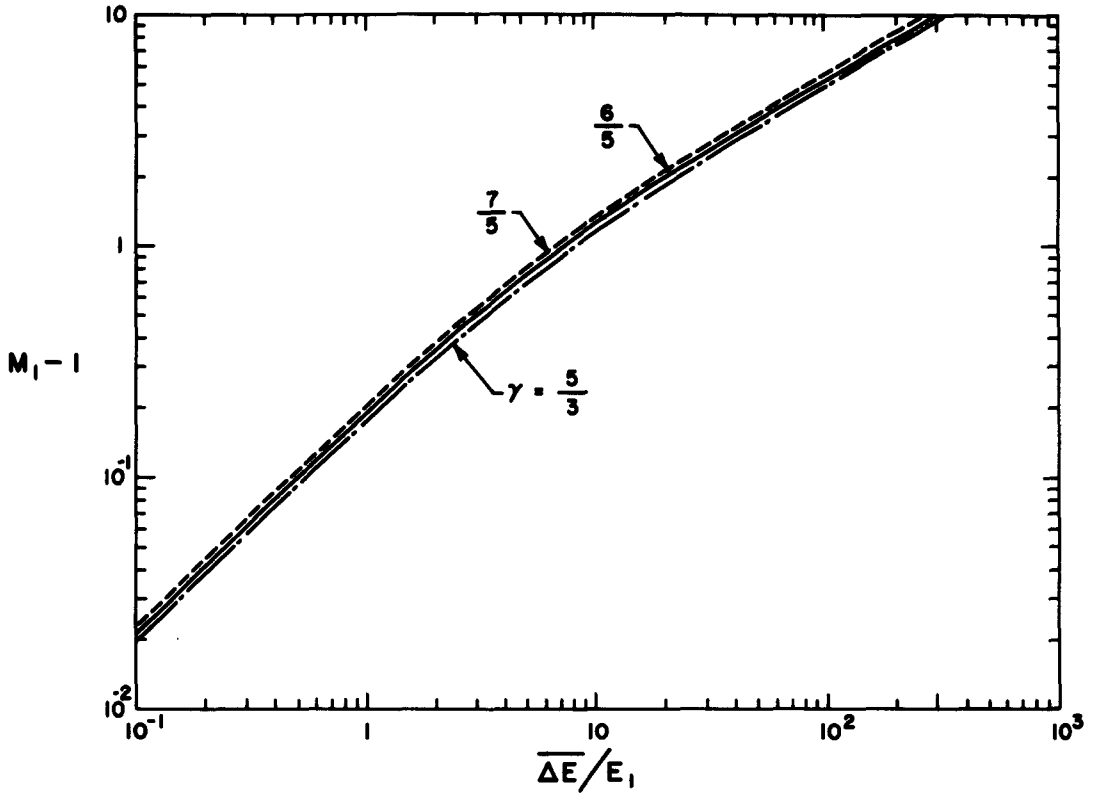

Fig. 1 Starting shock strength due to a sudden deposition of energy ΔE in a finite segment of gas of constant specific heats (γ = Cp/Cv) in a continuous one-dimensional channel of arbitrary cross-section. E_1 is the initial internal energy of the gas in the same segment and M_1 is the shock Mach number (i.e., the speed of the shock wave divided by the speed of sound of the undisturbed gas ahead of the shock) immediately after the energy deposition.

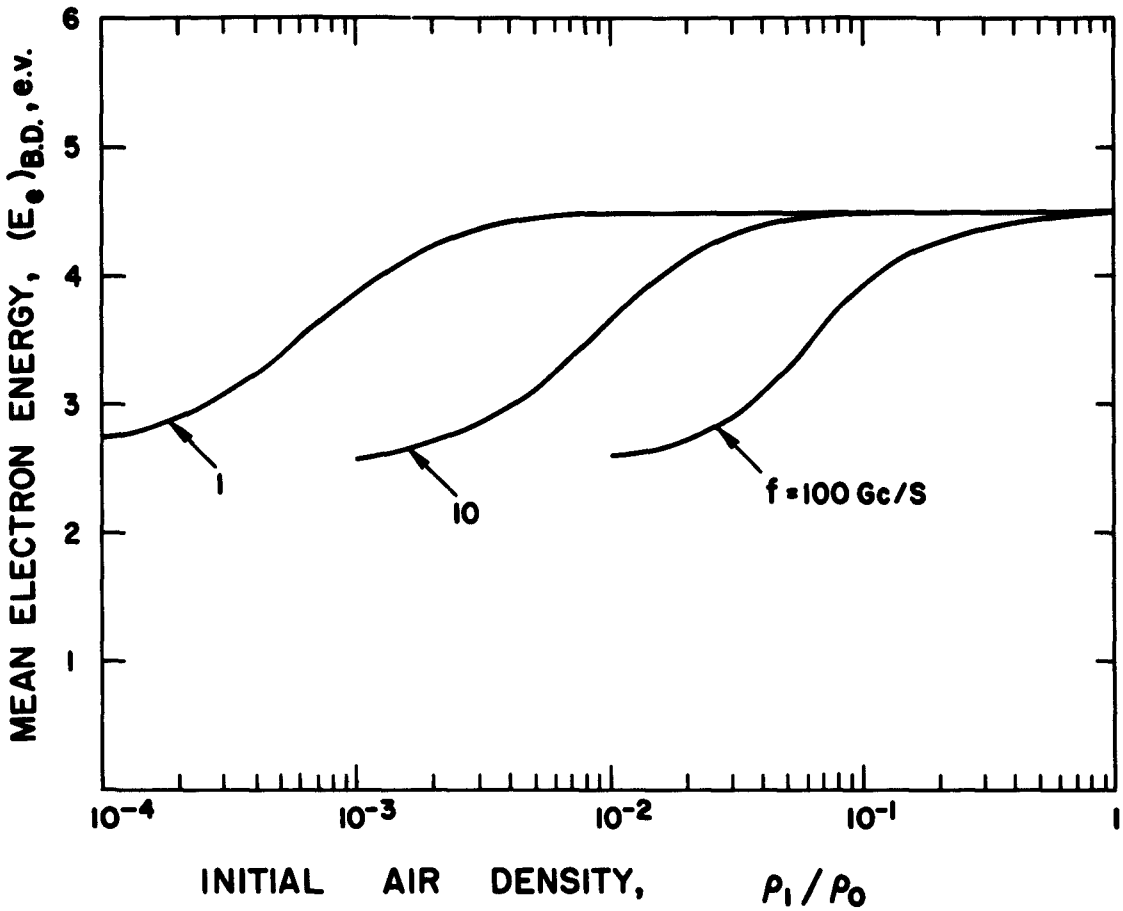

Fig. 2 Mean electron energy at minimum breakdown power density as a function of initial air density and frequency (1 Gc/S = 10^9 cycles/sec). The minimum breakdown condition is defined by Eq. (9), with $\eta_e = 0$. These results are obtained from Margenau's zeroth-order electron energy distribution and molecular data summarized in Appendix A.

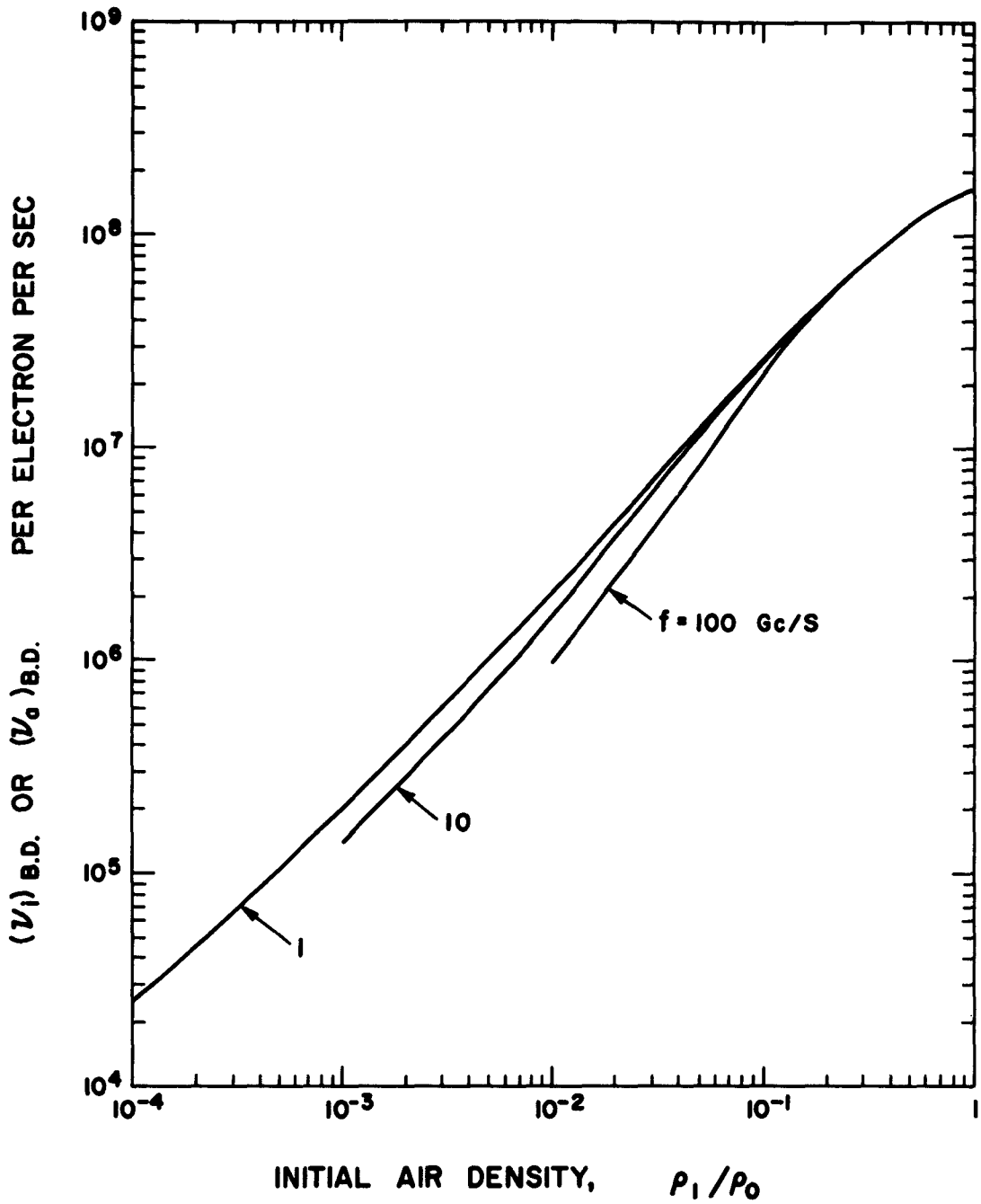

Fig. 3 Ionizing collision frequency (or electron attachment frequency) at minimum breakdown power density as a function of initial air density and frequency.

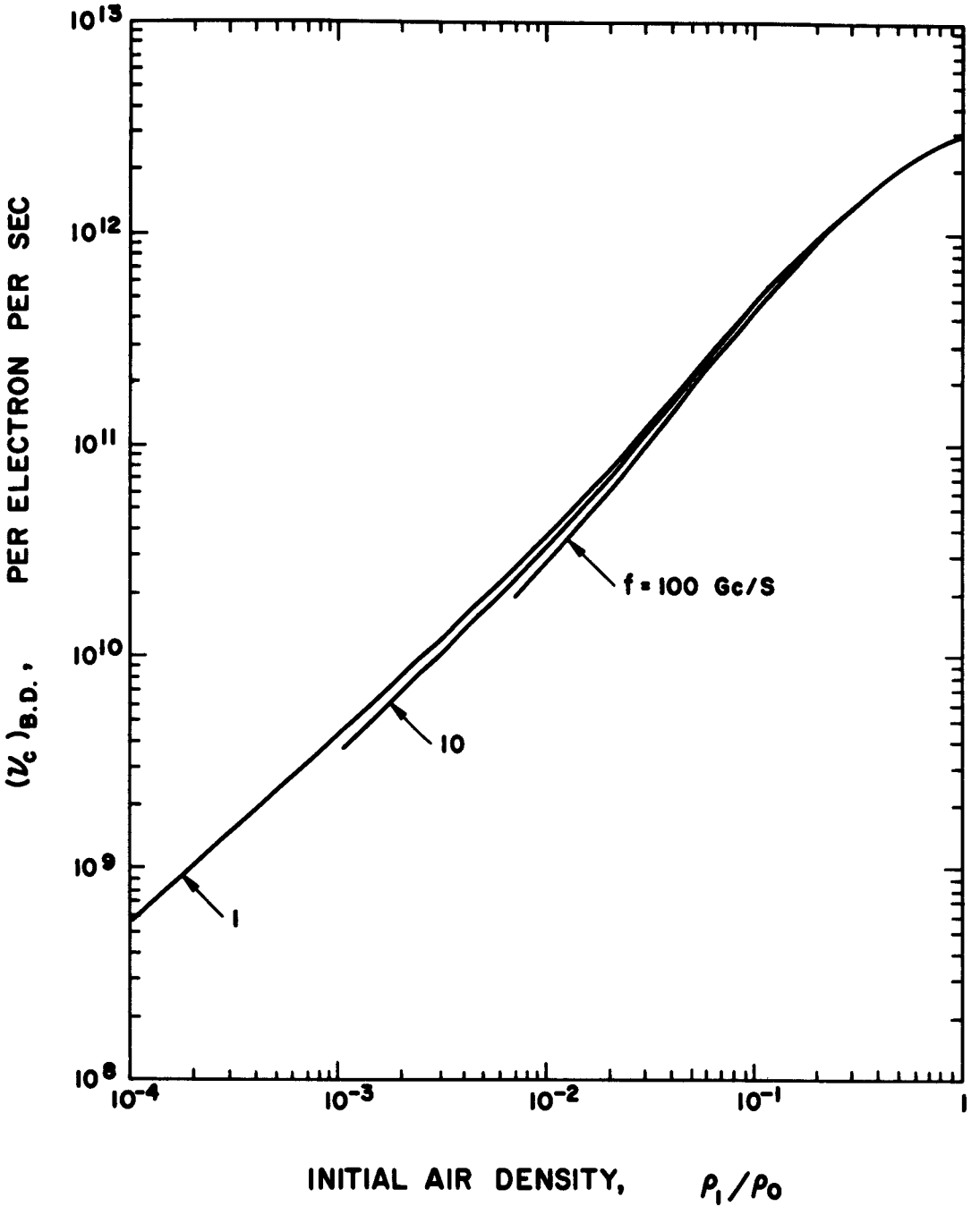

Fig. 4 Total collision frequency at breakdown as a function of initial air density and frequency.

9898

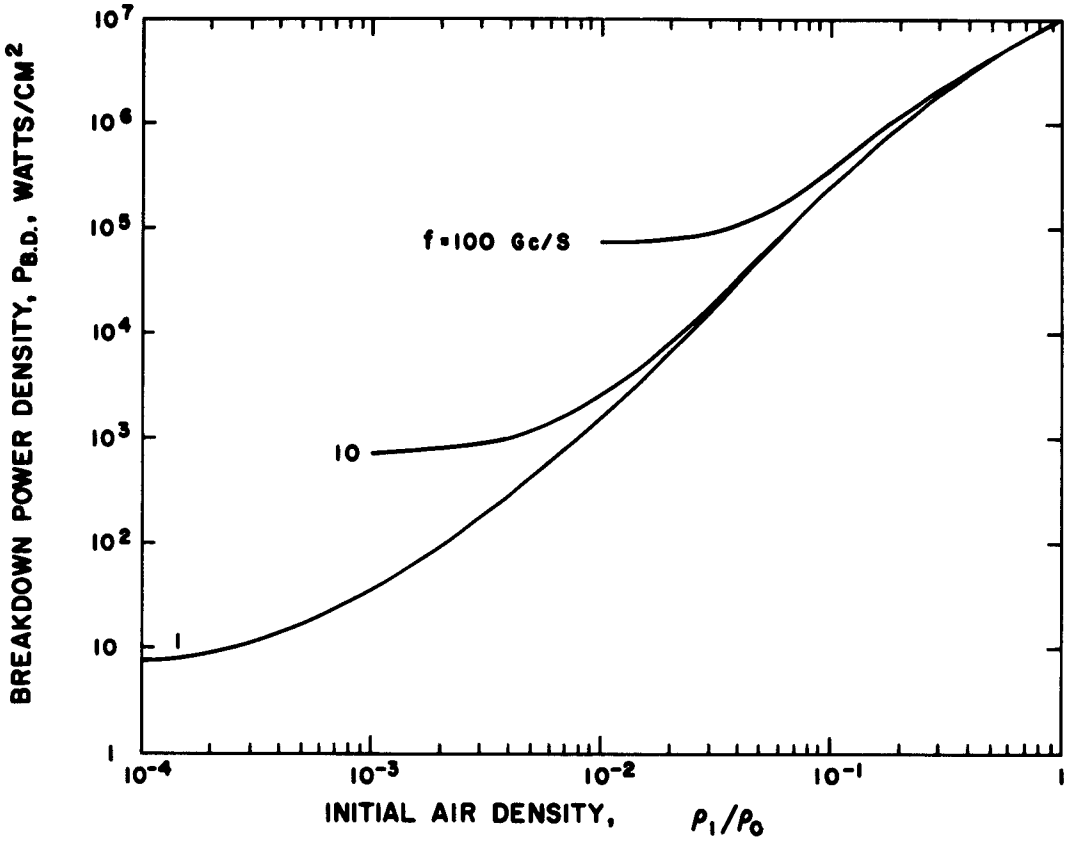

Fig. 5 Minimum breakdown power density as a function of initial air density and frequency.

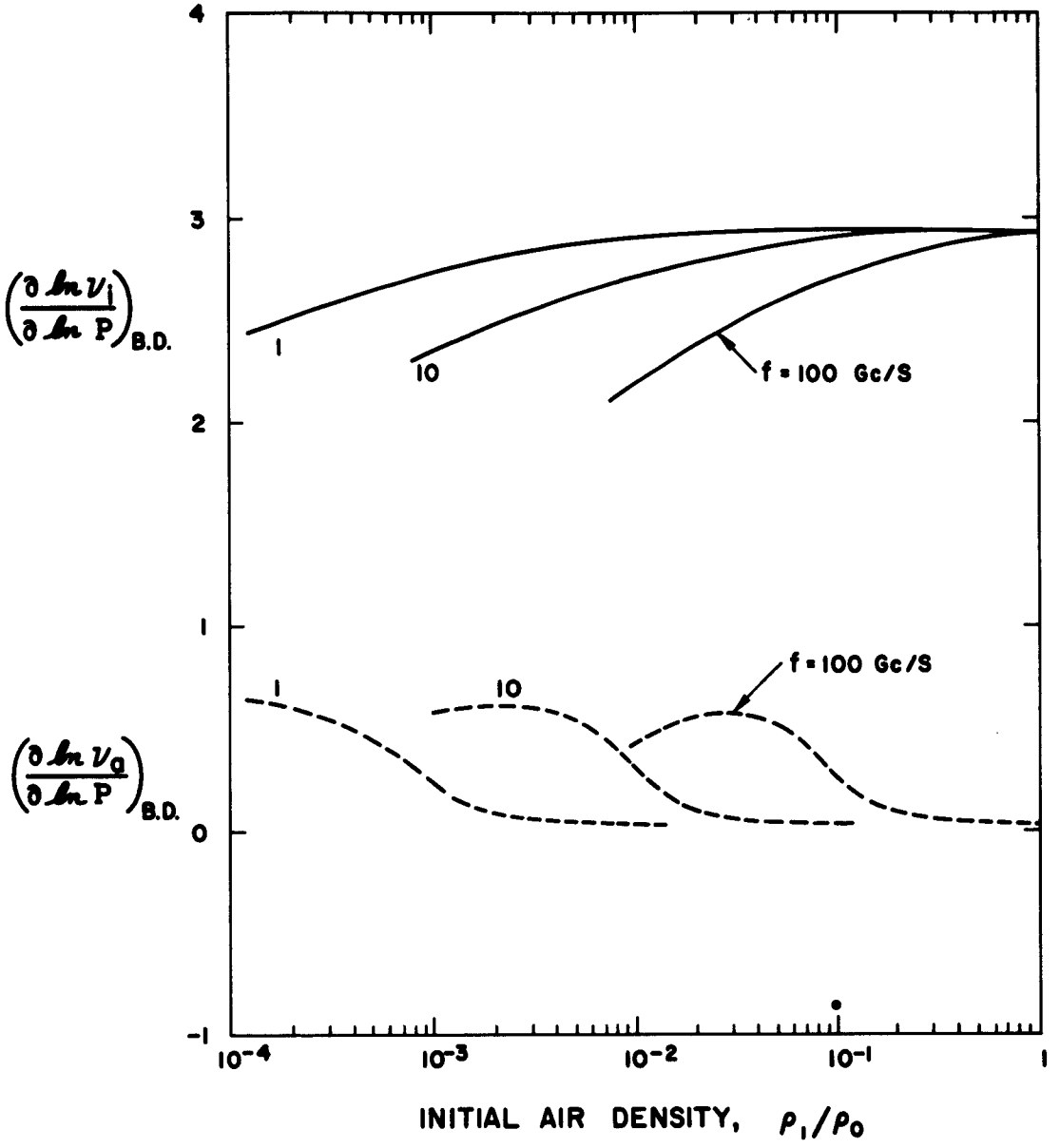

Fig. 6 Logarithmic derivatives of the ionizing collision frequency and of the electron attachment frequency with respect to microwave power density. These derivatives are evaluated at the minimum breakdown power density shown in Fig. 5.

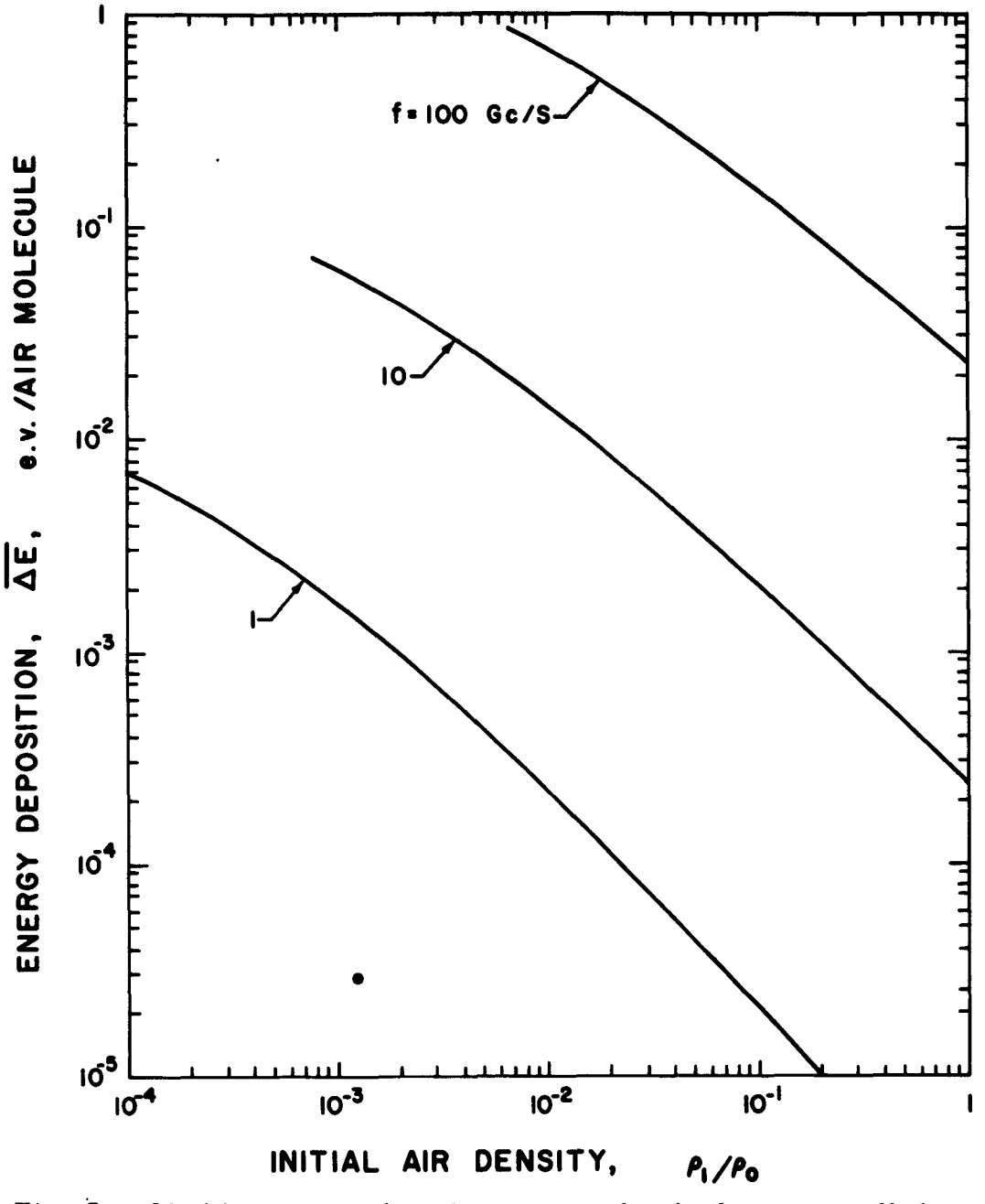

Fig. 7 Limiting energy deposition per molecule for uncontrolled microwave breakdown in air as a function of initial density and frequency. This quantity is calculated from Eq. (12), using mean electron energy and collision frequencies shown in Figs. 2, 3, 4 and energy loss coefficient Λ represented by the dotted curve in Fig. A1.

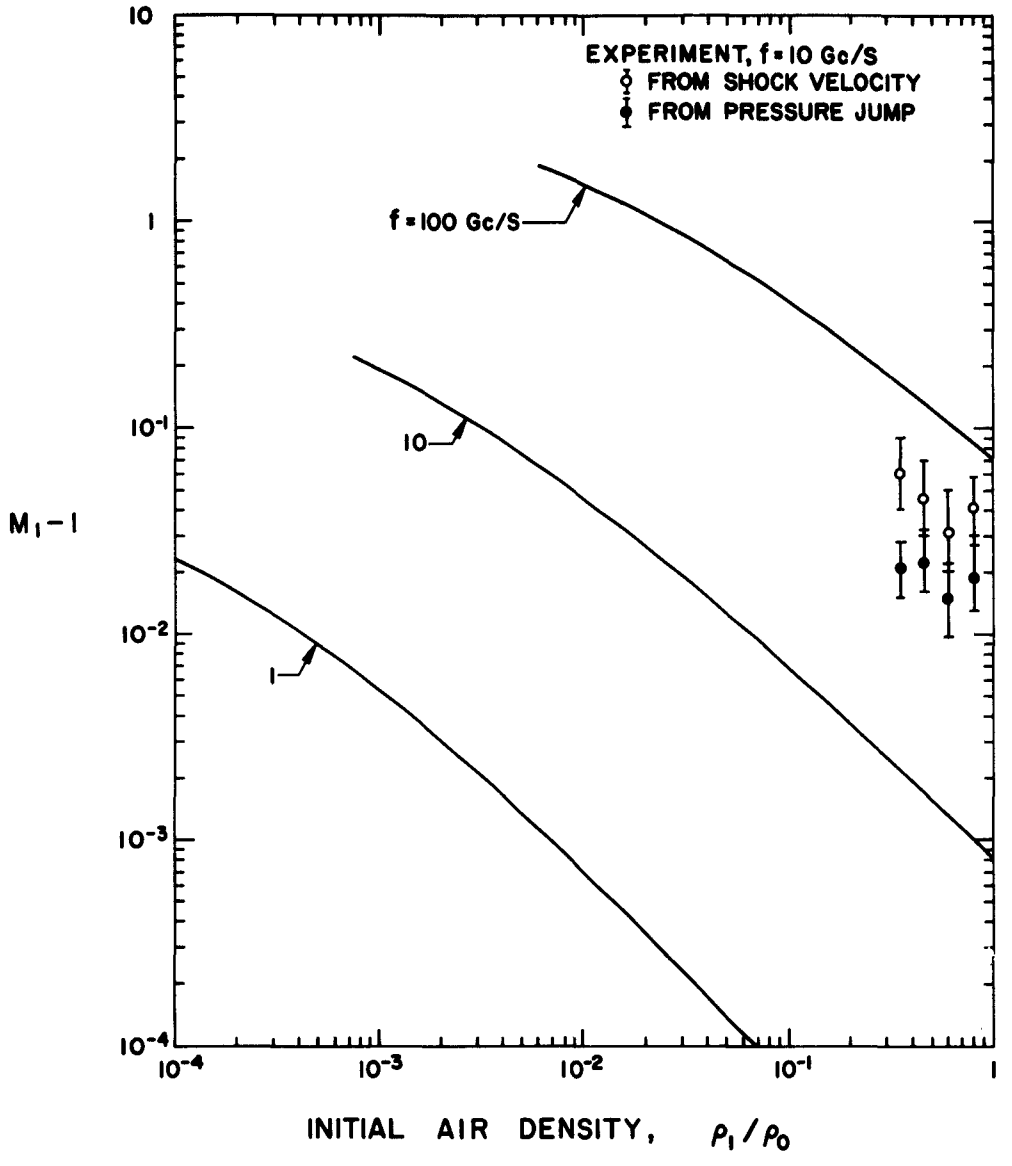

Fig. 8 Starting shock strength for uncontrolled microwave breakdown in air as a function of initial density and frequency. The theoretical curves are calculated from Eq. (1), using values of ΔE plotted in Fig. 7 and taking $\gamma = 7/5$, $E_1 = 6.3 \times 10^{-2}$ ev/molecule. The experimental points are obtained from preliminary experiment described in Section IV.

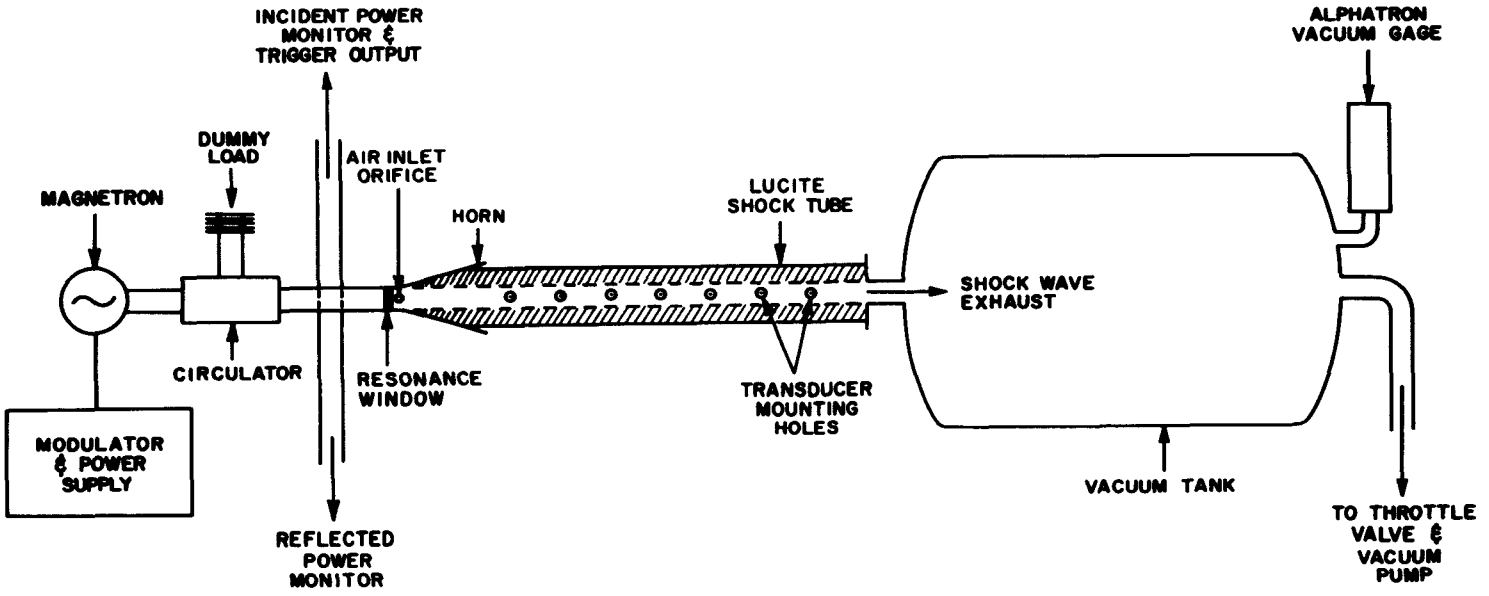

Fig. 9 Schematic drawing showing experimental arrangement for observation of pressure waves produced by pulse microwave discharges in a one-dimensional channel.

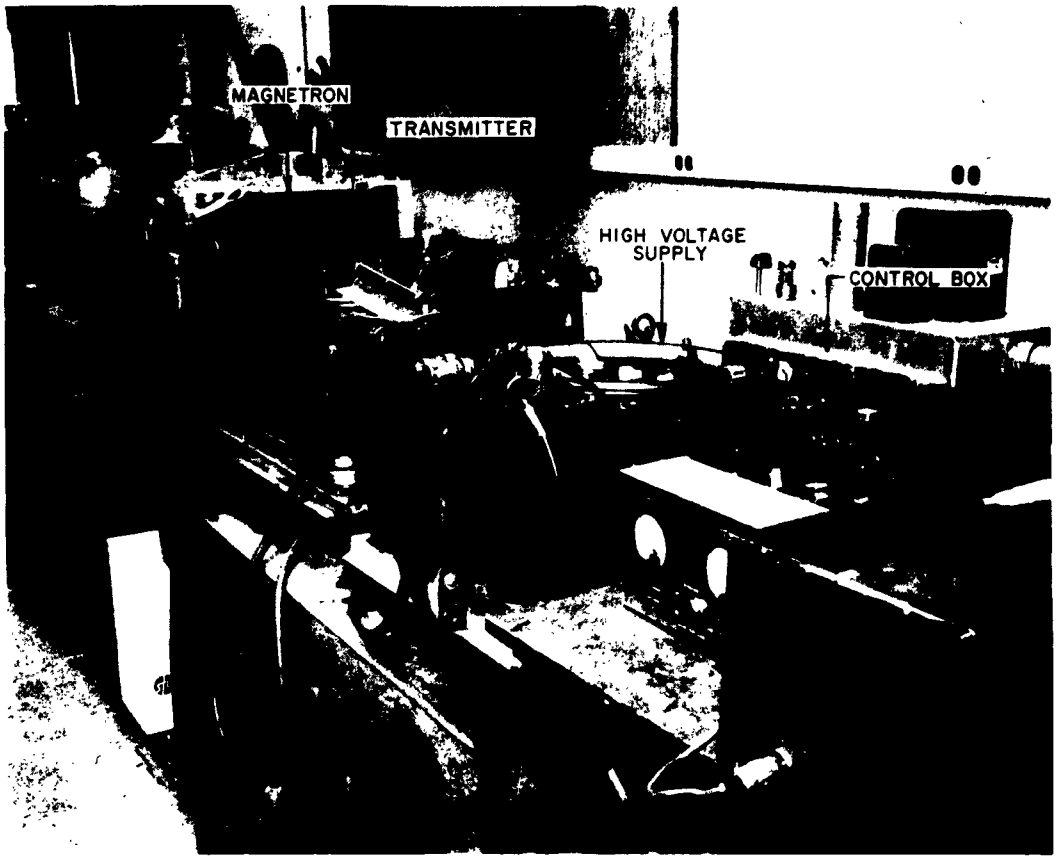

Fig. 10 (a), Photograph of experimental arrangement for observation of pressure waves produced by pulse microwave discharges in a one-dimensional channel.

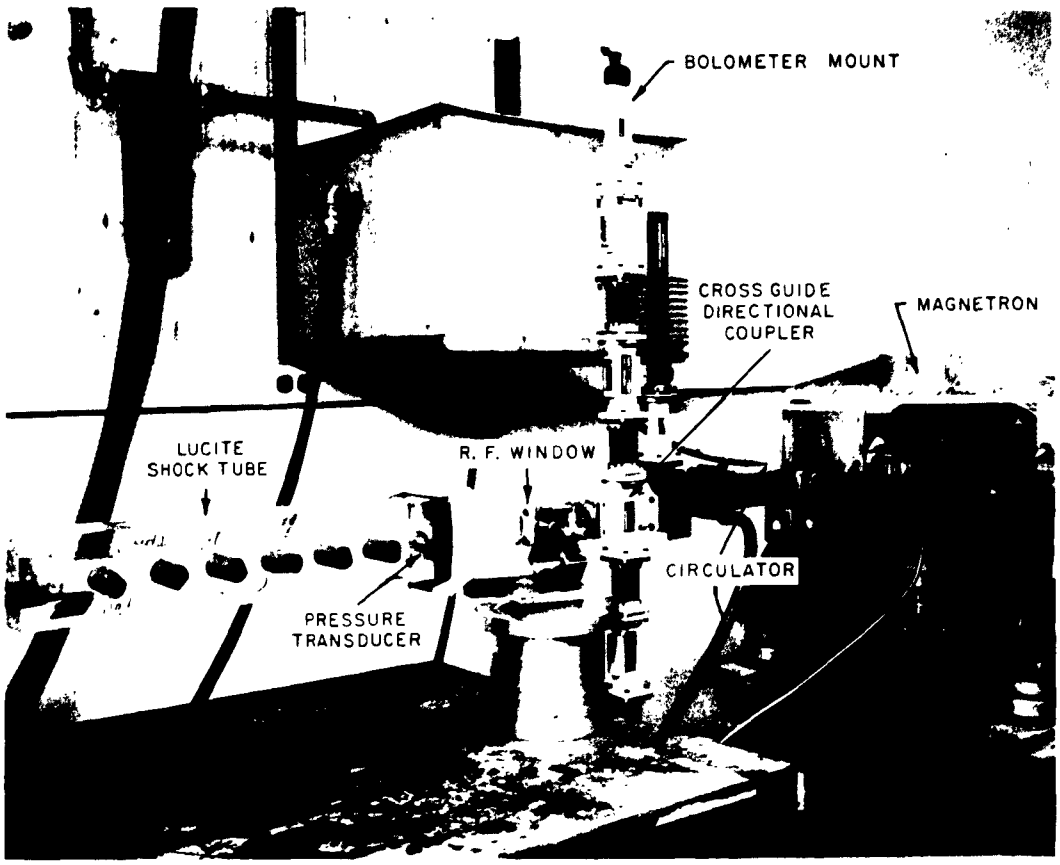

Fig. 10 (b) Photograph of experimental arrangement for observation of pressure waves produced by pulse microwave discharges in a one-dimensional channel.

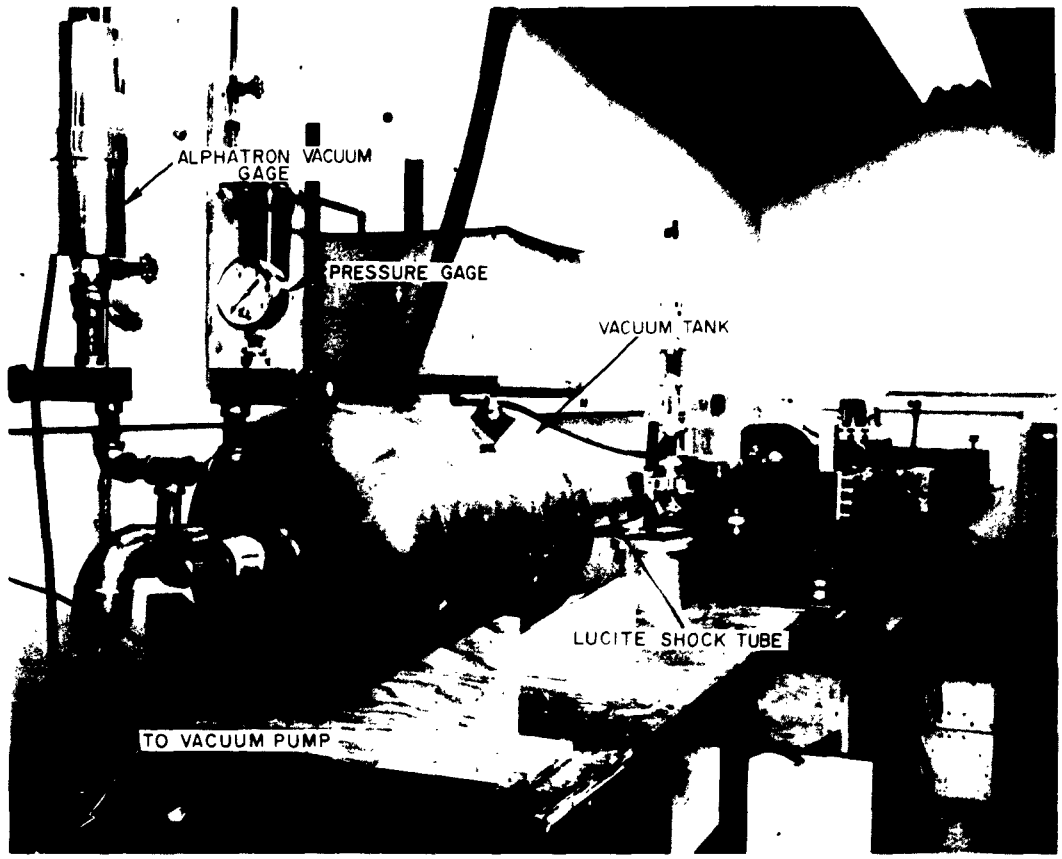

Fig. 10 (c) Photograph of experimental arrangement for observation of pressure waves produced by pulse microwave discharges in a one-dimensional channel.

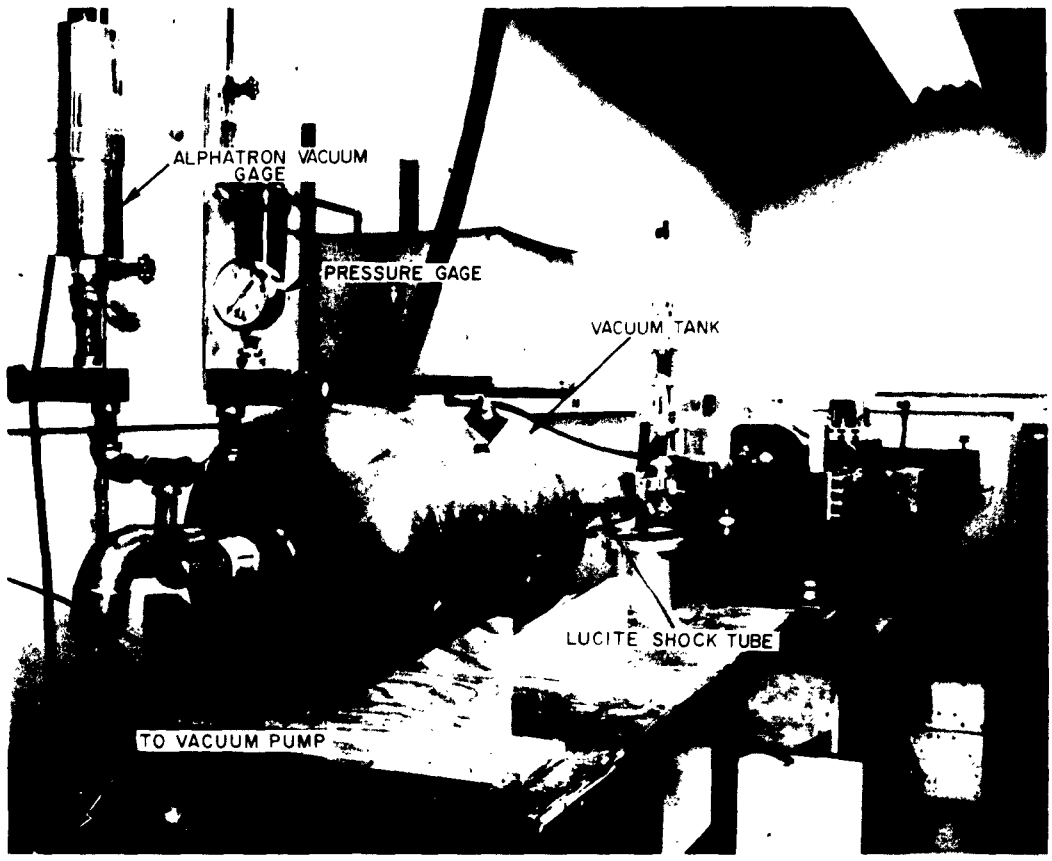

Fig. 10 (c) Photograph of experimental arrangement for observation of pressure waves produced by pulse microwave discharges in a one-dimensional channel.

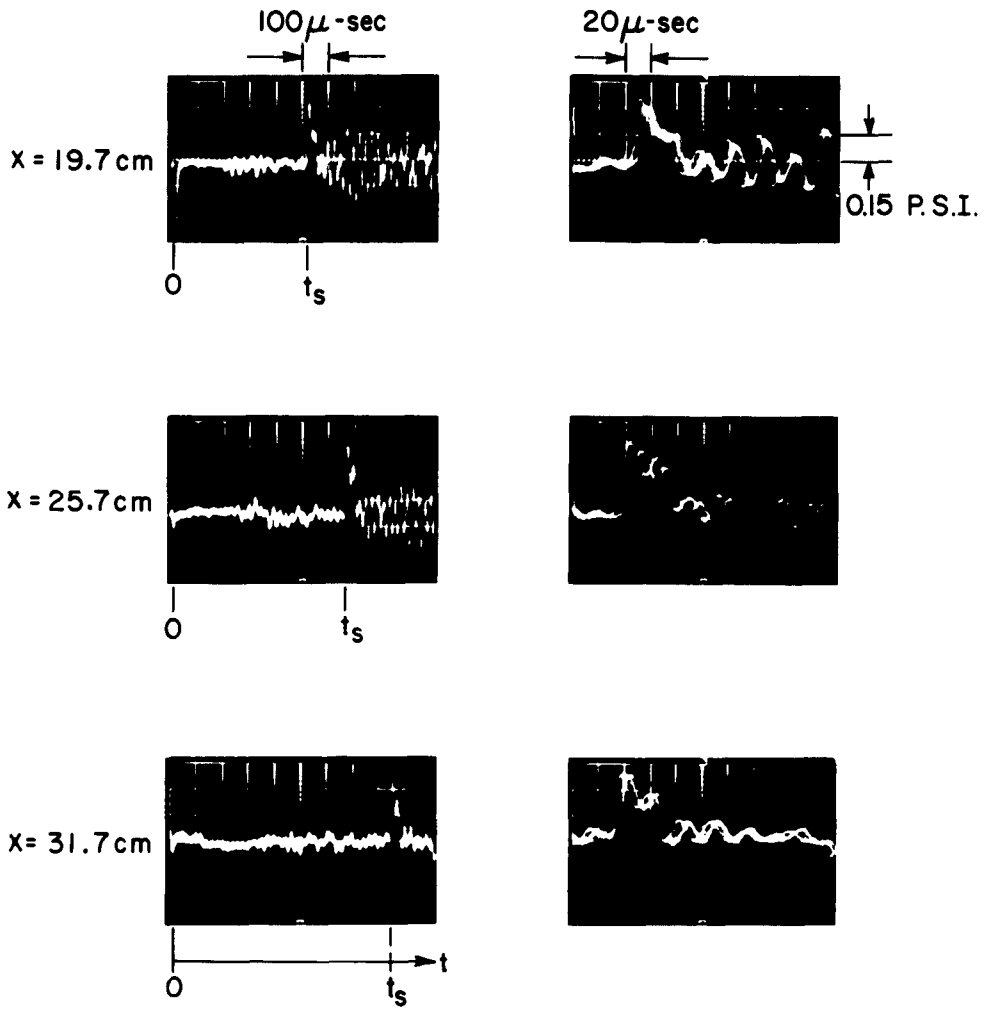

Fig. 11 (a) Typical oscillograms of pressure transducer output obtained at different axial distances x downstream of resonance window, where the microwave breakdown took place (see Fig. 9). The left hand oscillograms were obtained by triggering the oscilloscope with the microwave pulses without time delay. The right hand oscillograms were delayed-triggered and taken at higher sweep speed to magnify the main pressure pulse, the leading edge of which is marked by the time t_s beneath each oscillogram on the left. The initial air pressure was 450 $\pm$ 50 mm Hg (i.e., $\rho_1/\rho_o \cong$ 0.6). The microwave pulses, of 10 G_c/S frequency, 2×10^5 watts peak power, and 2 μ-sec duration, were repeated at the rate of 200 pulses/sec.

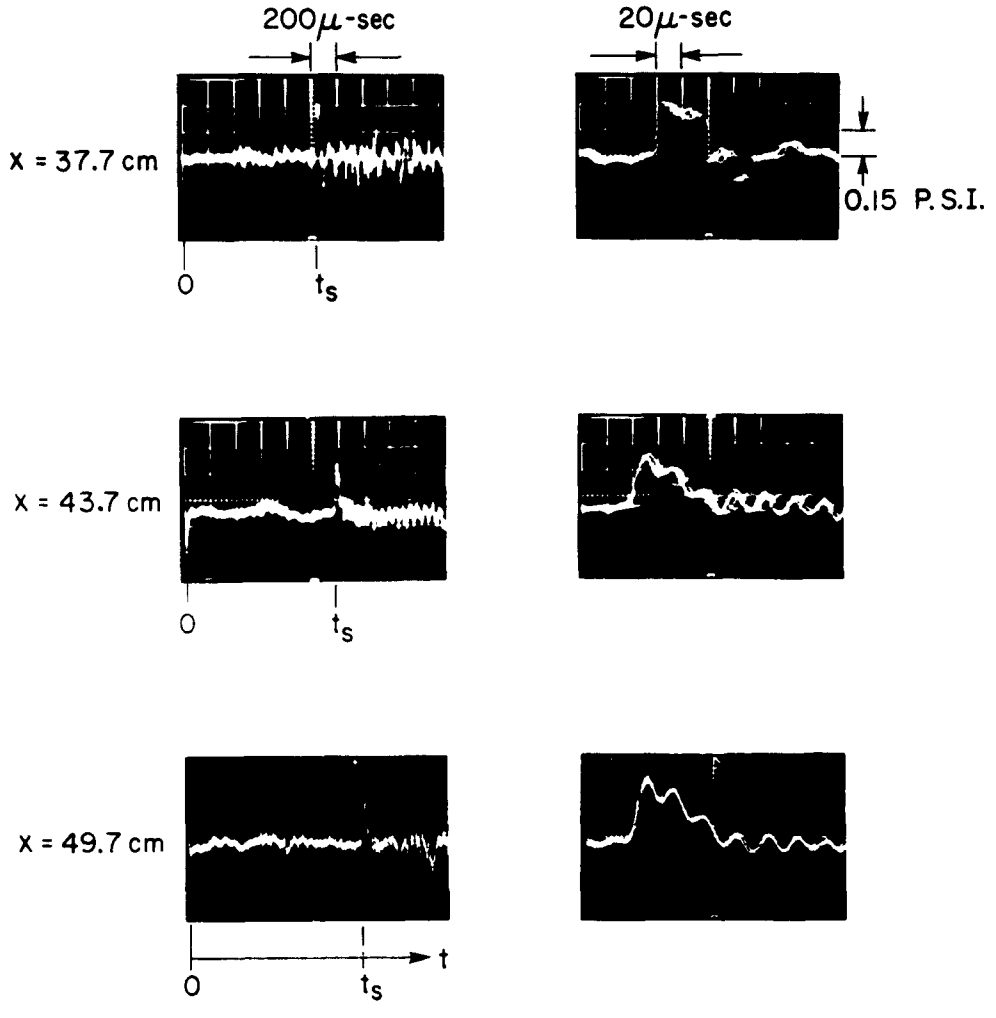

Fig. 11 (b) Typical oscillograms of pressure transducer output obtained at different axial distances x downstream of resonance window, where the microwave breakdown took place (see Fig. 9). The left hand oscillograms were obtained by triggering the oscilloscope with the microwave pulses without time delay. The right hand oscillograms were delayed-triggered and taken at higher sweep speed to magnify the main pressure pulse, the leading edge of which is marked by the time t_s beneath each oscillogram on the left. The initial air pressure was 450 $\pm$ 50 mm Hg (i.e., $\rho_1/\rho_o \cong 0.6$). The microwave pulses, of 10 G_c/S frequency, 2×10^5 watts peak power, and 2 μ-sec duration, were repeated at the rate of 200 pulses/sec.

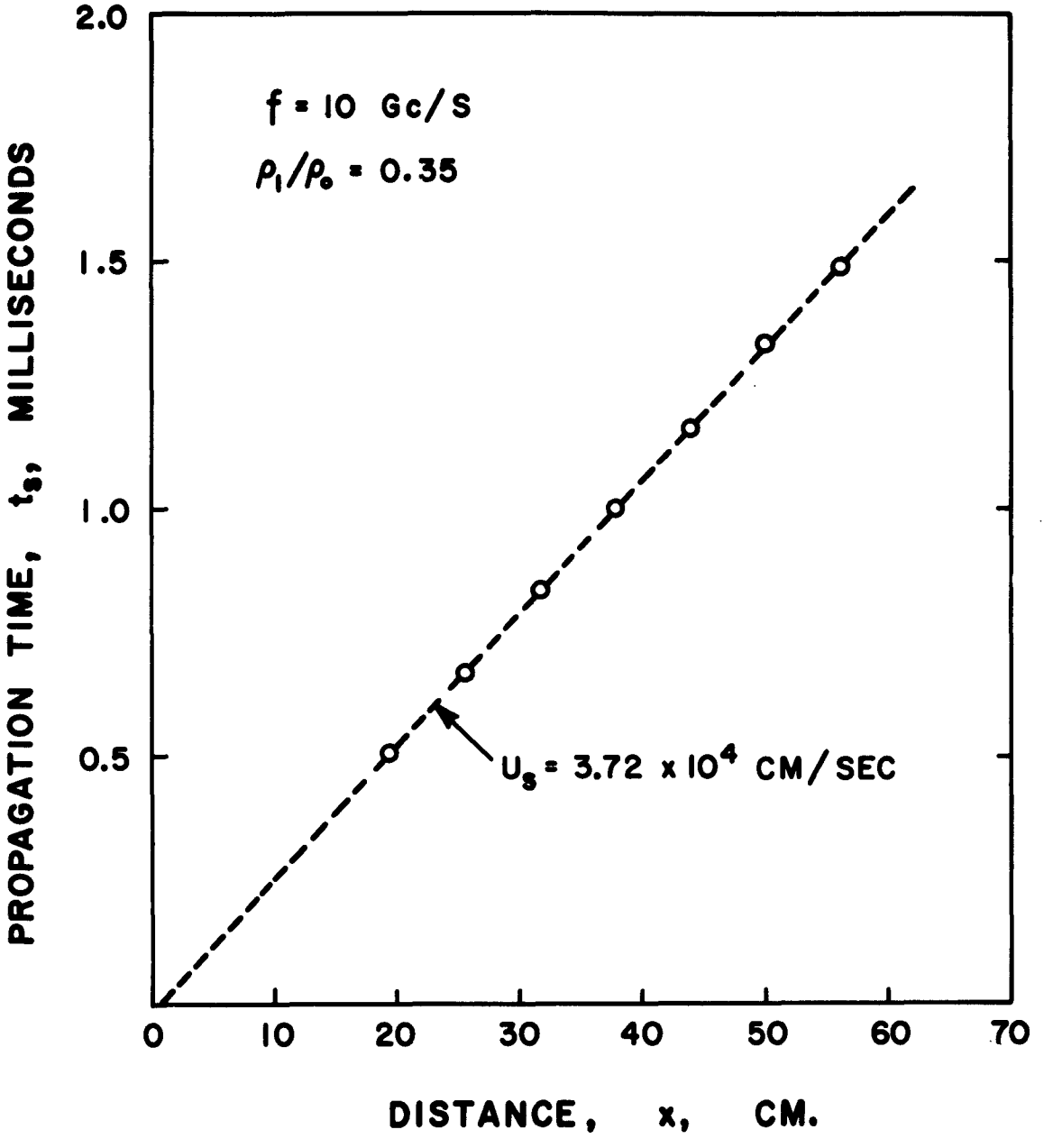

Fig. 12 A typical plot of the time of arrival of the main pressure pulse t_s as a function of axial distance x between the pressure transducer and the breakdown zone (see Fig. 11). A straight line fit of the experimental points indicates a propagation velocity of about 3.72 x 10^4 cm/sec in this case.

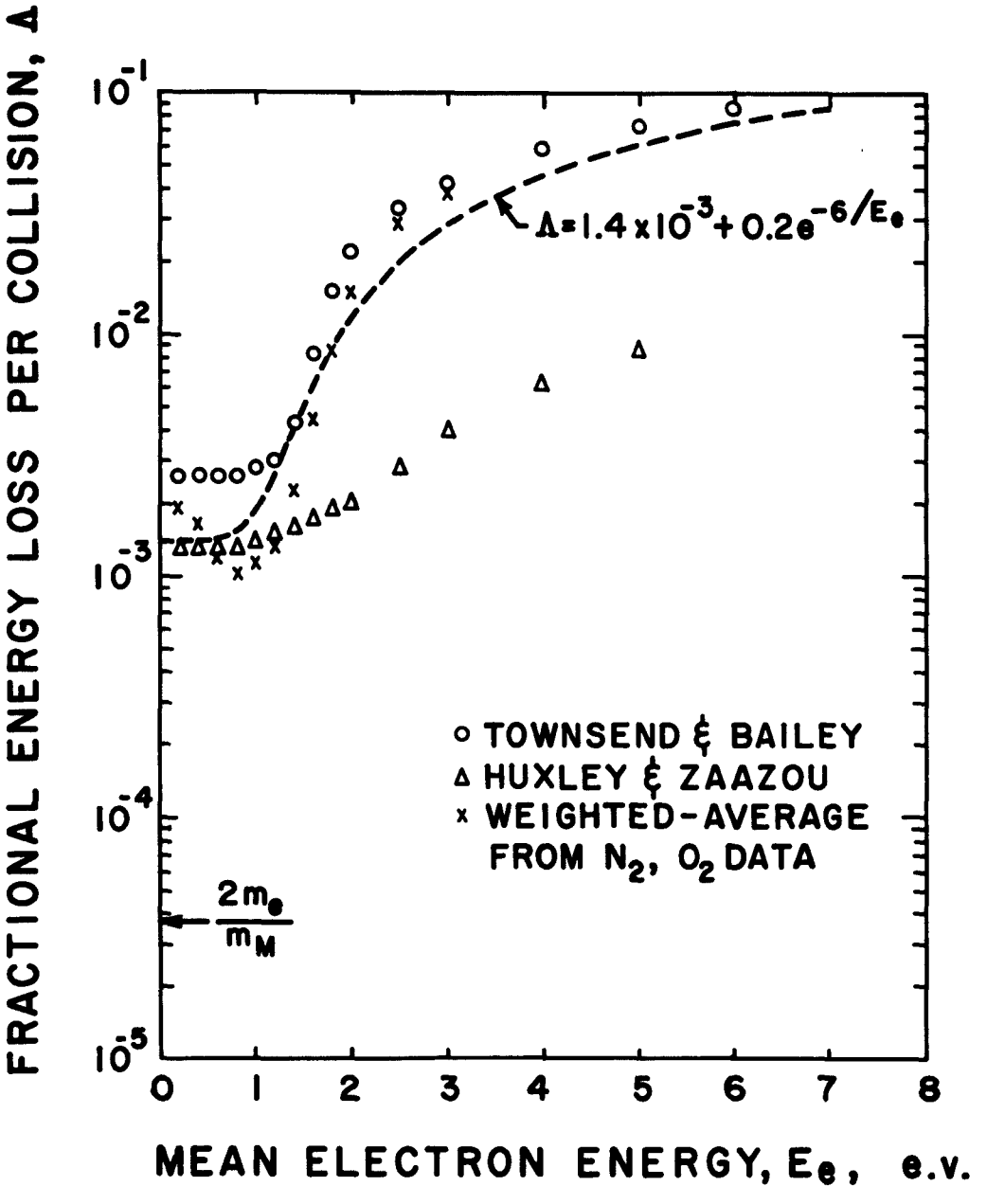

Fig. A1 Average fractional energy loss Λ due to collisions with air molecules of electrons of different mean energy E_e according to different investigators (from Table VI, p. 279 of Ref. 6). The value of Λ chosen for the present breakdown calculation is that represented by the dotted curve.

6888

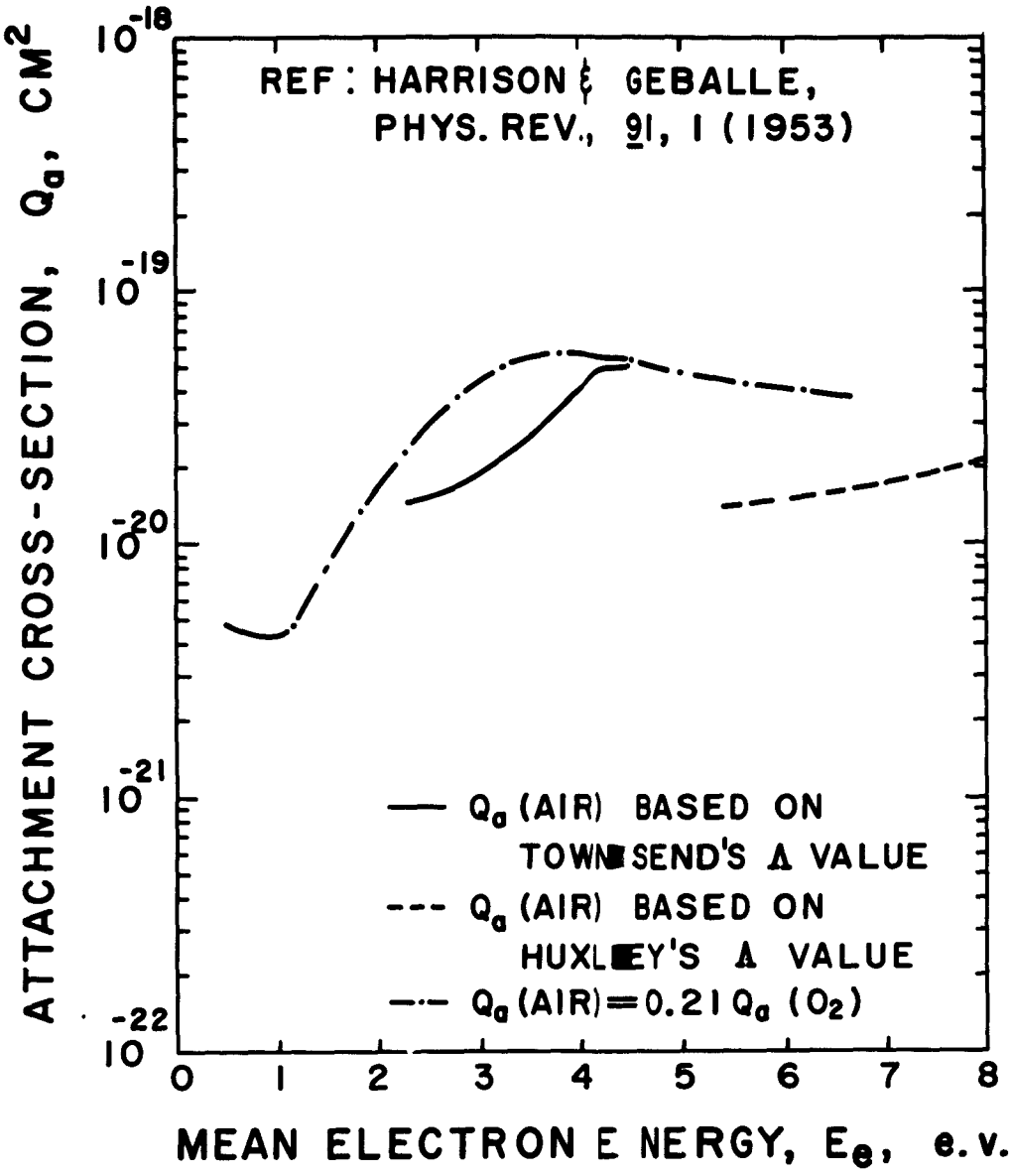

Fig. A2 Electron attachment cross section in air as a function of electron energy according to Harrison and Gaballe (Ref. 11). The value of Q_a chosen for the present calculation is that deduced from the O_2 measurement (dash-dot curve).

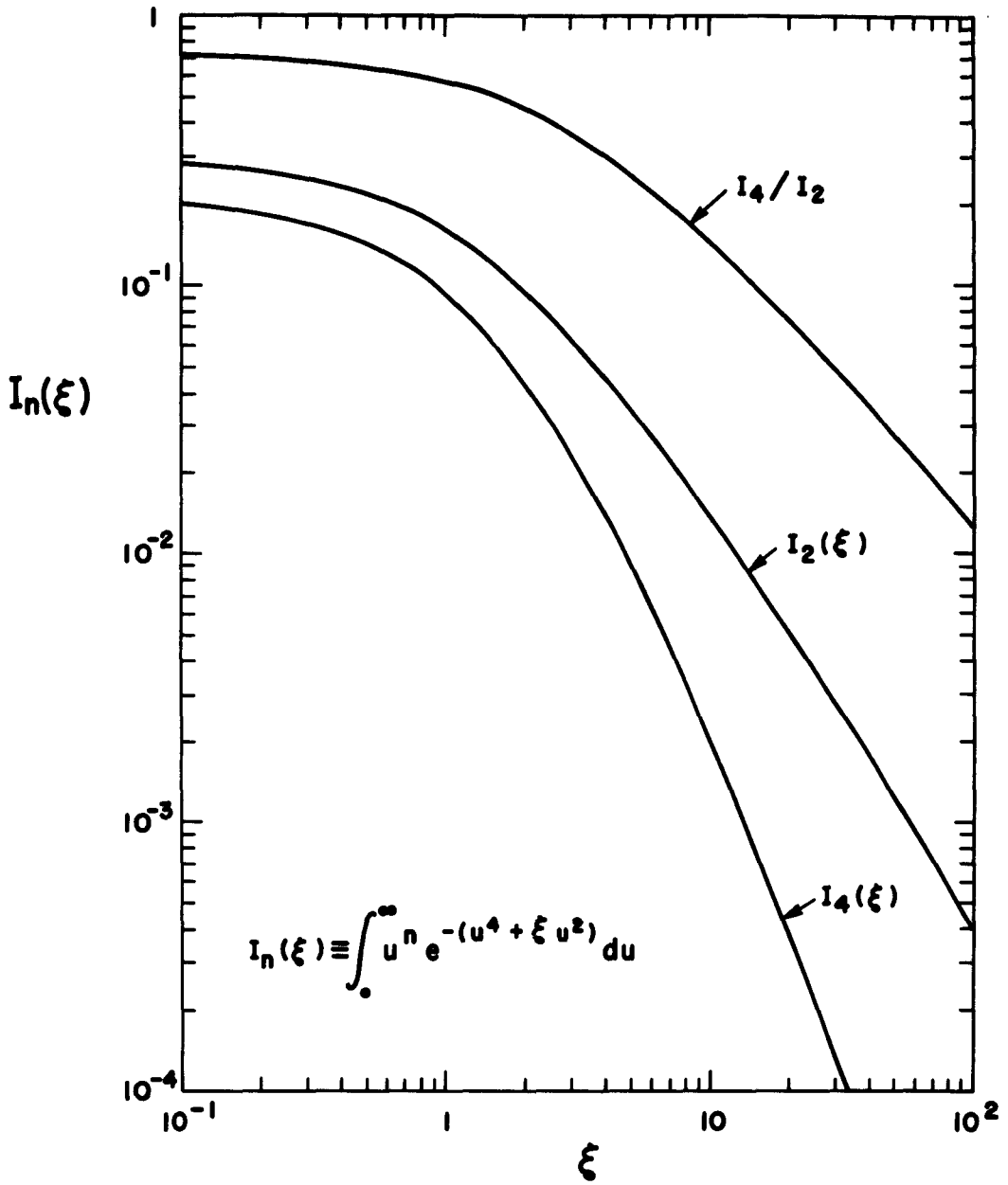

Fig. A3 Numerical value of the non-dimensional collision integrals $I_2(\xi)$ and $I_4(\xi)$ defined by Eqs. (A10) and (A12).

9894

DISTRIBUTION LIST
(List A)

AF 5 - AFMTC (AFMTC Tech Library - MU-135) - Patrick AFB, Fla. - (for unclassified material) - (1 copy)

AF 18 - AUL - Maxwell AFB, Ala. - (1 copy)

AF 32 - OAR (RROS, Col. John R. Fowler) - Tempo D - 4th and Independence Ave, Wash. 25, D.C. - (1 copy)

AF 33 - AFOSR, OAR (SRYP) - Tempo D - 4th and Independence Ave, Wash. 25, D.C. - (1 copy)

AF 43 - ASD (ASAPRD - Dist) - Wright-Patterson AFB, Ohio - (1 copy)

AF 124 - RADC (RAALD) - Griffiss AFB - New York - Attn: Documents Library - (1 copy)

AF 139 - AF Missile Development Center (MDGRT) - Holloman AFB, New Mexico - (1 copy)

AF 314 - Hq. OAR (RROSP, Maj. Richard W. Nelson) - Wash. 25, D.C. - (1 copy)

AF 318 - Aero Res. Lab. (OAR) - AROL Lib. AFL 2292, Bldg. 450 - Wright-Patterson AFB, Ohio - (1 copy)

Ar 5 - Commanding General - USASRDL - Ft. Monmouth, N.J. - Attn: Tech. Doc. Ctr. - SIGRA/SL-ADT - (1 copy)

Ar 9 - Department of the Army - Office of the Chief Signal Officer - Wash. 25, D.C. - Attn: SIGRD-4a-2 - (1 copy)

Ar 50 - Commanding Officer - Attn: ORDTL-012, Diamond Ordnance Fuze Laboratories, Wash. 25, D.C. - (1 copy)

Ar 67 - Redstone Scientific Information Center - U.S. Army Missile Command - Redstone Arsenal, Alabama - (1 copy)

G 2 - ASTIA (TIPAA) - Arlington Hall Station - Arlington 12, Virginia - (10 copies)

G 31 - Office of Scientific Intelligence - Central Intelligence Agency, 2430 E. Street, N.W., Wash. 25, D.C. - (1 copy)

G 68 - Scientific and Technical Information Facility - Attn: NASA Representative (S-AK/DL) - P.O. Box 5700 - Bethesda, Md. - (1 copy)

G 109 - Director - Langley Research Center - National Aeronautics and Space Administration - Langley Field, Virginia - (1 copy)

M 6 - AFCRL, OAR (CRXRA - Stop 39) - L.G. Hanscom Field, Bedford, Mass. (10 copies) (Please mail separately from any other reports going to this Hqs. as they must be sent to our Documents Section.)

M 84 - AFCRL, OAR (CRXR, J. R. Marple) L. G. Hanscom Field, Bedford, Mass. - (1 copy)

N 9 - Chief, Bureau of Naval Weapons - Department of the Navy - Washington 25, D.C. - Attn: DLI-31 - (1 copy)

N 29 - Director (Code 2027) - U. S. Naval Research Laboratory - Washington 25, D. C. - (1 copy)

I 292 - Director, USAF Project RAND - The Rand Corporation - 1700 Main Street, Santa Monica, Cal. - Thru: A.F. Liaison Office - (1 copy)

AF 253 - Technical Information Office - European Office - Aerospace Research - Shell Building - 47 Cantersteen - Brussels, Belgium - (1 copy)

Ar 107 - U.S. Army Aviation Human Research Unit - U.S. Continental Army Command - P.O. Box 428, Fort Rucker, Ala. Attn: Maj. Arne H. Eliasson - (1 copy)

G 8 - Library - Boulder Laboratories - National Bureau of Standards - Boulder, Colorado - (1 copy)

M 63 - Institute of the Aerospace Sciences, Inc. - 2 East 64th Street - New York 21, New York - Attn: Librarian - (1 copy)

N 73 - Office of Naval Research - Branch Office, London - Navy 100 - Box 39 - F.P.O. New York, N. Y. - (1 copy)

U 32 - Massachusetts Institute of Technology - Research Laboratory of Electronics - Building 26, Room 327 - Cambridge 39, Mass. - Attn: John H. Hewitt - (1 copy)

U 431 - Alderman Library - University of Virginia - Charlottesville, Virginia - (1 copy)

(List B-Q)

G 9 - Defence Research Member - Canadian Joint Staff - 2450 Massachusetts Ave., N. W. - Washington 8, D.C. - (- copy)

AF 68 - ASD (ASRNRE-3, Mr. Paul Springer) - Wright-Patterson AFB, Ohio - (1 copy)

AF 309 - RADC (RCWEC, Mr. Gerald Levy) - Griffiss AFB, N. Y. - (1 copy)

AF 316 - ARL (ARN) - Building 450 - Wright-Patterson AFB, Ohio - (1 copy)

AF 333 - AFBMD (Col. Donald Stine) - Air Force Unit Post Office - Los Angeles 45, California - (1 copy)

AF 334 - ASD (ASZR, Capt. G. W. S. Abbey) - Dynasoar WESPO Office - Wright-Patterson AFB, Ohio - (1 copy)

AF 335 - Hq. ASD (ASRNGE-2, D. A. Guidice) - Wright-Patterson AFB, Ohio - (1 copy)

AF 336 - ASD (ASRMDF - 3, Mr. G. W. Riese) - Wright-Patterson AFB, Ohio - (1 copy)

Ar 112 - Commanding Officer - Diamond Ordnance Fuse Laboratories - Wash. 25, D.C. - Attn: Dr. R. E. Bowles - (1 copy)

Ar 113 - Commanding Officer - Diamond Ordnance Fuse Laboratories - Wash. 25, D.C. - Attn: Mrs. Ruth N. Ryan - Library - (1 copy)

G 98 - U.S. Atomic Energy Commission - Office of Technical Information Extension - P.O. Box 62 - Oak Ridge, Tennessee - (1 copy)

G 115 - NASA (Mr. Michael C. Ellis) - Langley Research Center - Hampton, Va. - (1 copy)

G 116 - NASA (Dr. R. V. Hess) - Langley Research Center - Hampton, Va. - (1 copy)

G 117 - NASA Instrument Research Division - Langley Research Center - Langley Field, Va - Attn: Mr. C. E. Green, Jr. - (1 copy)

G 118 - NASA Flight Research Center - Box 273 - Edwards, Calif. - Attn: John J. Bernard - (1 copy)

I 737 - The Hallicrafters Co. - 5th and Kostner Aves. - Chicago 24, Ill. - Attn: Henri Hodara - Head of Space Communication - (1 copy)

I 781 - RCA Victor Co., Ltd. - Research Laboratories - 1001 Lenoir St. - Montreal, P. Q., Canada - Attn: Dr. M. P. Bachynski - (1 copy)

I 893 - General Electric Co. - 3750 D Street - Philadelphia 24, Pa. - Attn: Mr. H. G. Lew - Missile and Space Vehicle Dept. - (1 copy)

I 938 - Avco-Everett Research Laboratory - 2385 Revere Beach Parkway - Everett 49, Mass. - Attn: Library - (1 copy)

I 940 - Aerospace Corp. - Box 95085 - Los Angeles 45, Calif. - Attn: Library - (1 copy)

I 958 - Aeronutronics - Division of Ford Motor Co. - Newport Beach, Calif. - Attn: Dr. Frank Dixon - 609A Systems Manager - (1 copy)

I 959 - Siena Research Corp. - P. O. Box 22 - Buffalo 25, New York - Attn: Mr. Herbert Mennen - (1 copy)

I 960 - Boeing Aircraft Co. - Seattle, Washington - Attn: Mr. John D. Kelly - (1 copy)

I 961 - Boeing Aircraft Co. - Seattle, Washington - Attn: Dr. George Tyras - Mail Stop 22-04 - (1 copy)

I 962 - Aerospace Corp. - Box 95085 - Los Angeles 45, Calif. - Attn: Howard King - (1 copy)

I 963 - General Electric Co. - 3750 D Street - Philadelphia 24, Pa. - Attn: Dr. W. King - (1 copy)

I 964 - Avco Research and Advanced Development - 201 Lowell St., Wilmington, Mass. - Attn: J. R. White, Section Chief - Advanced Communications, Electronics and Electromechanics Department - (1 copy)

I 965 - The Bendix Corporation, Bendix Systems Division - 3300 Plymouth Road, Ann Arbor, Michigan - Attn: C. M. Shoar - (1 copy)

I 966 - Cornell Aeronautical Lab., Inc. - Buffalo, New York - Attn: Mr. A. Hertzberg - (1 copy)

I 968 - General Applied Science Lab., Inc. - Merrick and Stewart Aves. - E. Meadow, New York - Attn: Dr. A. Ferri - (1 copy)

I 969 - General Applied Science Lab. Inc. - Merrick and Stewart Aves. - E. Meadow, New York - Attn: Dr. M. Abele - (1 copy)

I 970 - Electronic Communications, Inc. - P. O. Box 12248 - St. Petersburg 33, Florida - Attn: Mr. M. R. Donaldson - Advanced Development Sec. - (1 copy) - (when report is classified, send to: 1501 72F Street, North)

I 971 - Page Communications Engineers, Inc. - 2001 Wisconsin Ave., N. W. - Washington 7, D. C. - Attn: Dr. L. P. Yeh - (1 copy)

I 972 - Philco Corporation - 3875 Fabian Way - Palo Alto, Calif. - Attn: Mr. D. W. Swayze - Western Development Labs. - Government and Industrial Div. - (1 copy)

I 973 - Republic Aviation Corp. - Farmingdale, New York - Attn: Mr. A. E. Kunen - Manager, Plasma Propulsion - (1 copy)

I 974 - Republic Aviation Corp. - Farmingdale, New York - Attn: Dr. Alex Grumet - Sci. Res. Staff, Dept. 64 - (1 copy)

I 975 - General Electric Company - P. O. Box 11 - Schenectady 5, New York - Attn: Mr. Peter P. Keenan - Building 27, Rm 478 - (1 copy)

I 976 - Hughes Aircraft Co. - Fullerton, Calif. - Attn: Mr. A. E. Geiger - Building 600/F-231 - (1 copy)

M 68 - AFCCDD (CCRAC-7 - Maj. W. Ambruster II) - L. G. Hanscom Field - Bedford, Mass. - (1 copy)

M 69 - CARDE - Valcartier, P. O. Q., - Canada - Attn: Dr. Gerry Bull - (1 copy)

N 162 - Commanding Officer - U. S. Naval Ordnance Laboratory - Corona, Calif. - Attn: Mr. Wes Seeley - (1 copy)

U 48 - Polytechnic Institute of Brooklyn - Microwave Research Institute - 55 Johnson St. - Brooklyn, New York - Attn: Dr. Arthur A. Oliner (1 copy)

U 222 - Massachusetts Institute of Technology - Lincoln Laboratory - P. O. Box 73 - Lexington 73, Mass. - Attn: Dr. S. Edelberg - Group 312 - (1 copy)

U 238 - University of Southern California - University Park - Los Angeles 7, Calif. - Attn: Z. A. Kaprielian - Associate Professor of Electrical Engineering - (1 copy)

U 362 - Massachusetts Institute of Technology - Lincoln Laboratory - P. O. Box 73 - Lexington 73, Mass. - Attn: Dr. G. Pippert - (1 copy)

U 418 - University of California - Los Angeles, Calif. - Attn: Prof. R. S. Elliot - (1 copy)

U 419 - Polytechnic Institute of Brooklyn - Freeport - New York - Attn: Prof. Roberto Vaglio-Laurin - Aerodynamics Lab. - (1 copy)

U 420 - University of Southern California - University Park - Los Angeles 7, Calif. - Attn: Dr. Hans Kuehl - Engineering Center - (1 copy)

U 421 - California Institute of Technology - Dept. of Electrical Engineering - Pasadena, Calif. - Attn: Prof. N. George, Jr. - (1 copy)

Remaining copies to: Hq. AFCRL, OAR (CRD) - L. G. Hanscom Field, Bedford, Mass. - (5 copies)

Avco-Everett Research Laboratory, Everett, Massachusetts
HYDRODYNAMIC EFFECTS PRODUCED BY PULSE MICROWAVE DISCHARGES, by S. C. Lin and G. P. Theofilos. October 1962. 43 p. incl. illus. (Project 5561; Task 556112)
(Avco-Everett Research Report 138; AFCRL-63-126)
(Contract AF 19(604)-7458)

Unclassified report

An elementary theory is developed for predicting the strength of pressure waves to be expected from sudden breakdown of a gas by high frequency electromagnetic waves in a one-dimensional geometry. It is shown that for an uncontrolled breakdown where the local field strength is not carefully matched to the instantaneous plasma condition to avoid strong reflections, the heating effect will be self-limiting and the resultant shock strength depends only on the incident wave frequency and on the initial gas density. Numerical example for microwave breakdown in air indicates that at normal sea level density, the shock wave

(over)

accompanying the breakdown is generally quite weak (of the order of Mach 1.1 at 100 Gc/S frequency). However, for breakdown at lower air densities, stronger shock waves can be anticipated. Preliminary experimental observations of pressure waves generated in a one-dimensional channel by pulse microwave discharges tended to confirm the general features of the elementary theory but showed somewhat stronger effects than predicted.

UNCLASSIFIED

1. Discharges, Microwave-Hydrodynamic effects.
2. Gases-Breakdown.
3. Shock waves.
I. Title.
II. Lin, S. C.
III. Theofilos, G. P.
IV. Avco-Everett Research Report 138.
V. AFCRL-63-126.
VI. Contract AF 19(604)-7458.

UNCLASSIFIED

UNCLASSIFIED

UNCLASSIFIED

Avco-Everett Research Laboratory, Everett, Massachusetts
HYDRODYNAMIC EFFECTS PRODUCED BY PULSE MICROWAVE DISCHARGES, by S. C. Lin and G. P. Theofilos. October 1962. 43 p. incl. illus. (Project 5561; Task 556112)
(Avco-Everett Research Report 138; AFCRL-63-126)
(Contract AF 19(604)-7458)

Unclassified report

An elementary theory is developed for predicting the strength of pressure waves to be expected from sudden breakdown of a gas by high frequency electromagnetic waves in a one-dimensional geometry. It is shown that for an uncontrolled breakdown where the local field strength is not carefully matched to the instantaneous plasma condition to avoid strong reflections, the heating effect will be self-limiting and the resultant shock strength depends only on the incident wave frequency and on the initial gas density. Numerical example for microwave breakdown in air indicates that at normal sea level density, the shock wave

(over)

accompanying the breakdown is generally quite weak (of the order of Mach 1.1 at 100 Gc/S frequency). However, for breakdown at lower air densities, stronger shock waves can be anticipated. Preliminary experimental observations of pressure waves generated in a one-dimensional channel by pulse microwave discharges tended to confirm the general features of the elementary theory but showed somewhat stronger effects than predicted.

UNCLASSIFIED

1. Discharges, Microwave-Hydrodynamic effects.
2. Gases-Breakdown.
3. Shock waves.
I. Title.
II. Lin, S. C.
III. Theofilos, G. P.
IV. Avco-Everett Research Report 138.
V. AFCRL-63-126.
VI. Contract AF 19(604)-7458.

UNCLASSIFIED

UNCLASSIFIED

UNCLASSIFIED